Title

ELECTRON SCATTERING BY METHANE. ELASTIC SCATTERING AND ROTATIONAL EXCITATION CROSS SECTIONS CALCULATED WITH Ab Initio INTERACTION POTENTIALS

Author

Abusalbi, N.

Publication Date

1982-07-01

NRCC NATIONAL RESOURCE FOR COMPUTATION IN CHEMISTRY

Submitted for publication in the Journal of Chemical Physics

ELECTRON SCATTERING BY METHANE. ELASTIC SCATTERING AND ROTATIONAL EXCITATION CROSS SECTIONS CALCULATED WITH *Ab Initio* INTERACTION POTENTIALS

Najib Abusalbi, Robert A. Eades, Tonny Nam, Devarajan Thirumalai, David A. Dixon, Donald G. Truhlar, and Michel Dupuis

July 1982

LAWRENCE BERKELEY LABORATORY
UNIVERSITY OF CALIFORNIA

Prepared for the U.S. Department of Energy under Contract DE-AC03-76SF00098 and for the National Science Foundation under Interagency Agreement CHE-7721305

DISCLAIMER

Electron Scattering by Methane. Elastic Scattering and Rotational Excitation Cross Sections Calculated with *Ab Initio* Interaction Potentials

Najib Abusalbi, Robert A. Eades, Tonny Nam,[a] Devarajan Thirumalai,[b]

David A. Dixon, and Donald G. Truhlar

Department of Chemistry and Chemical Physics Program
University of Minnesota
Minneapolis, Minnesota 55455

and Michel Dupuis[c]

National Resource for Computation in Chemistry
Lawrence Berkeley Laboratory, University of California,
Berkeley, California 94720

[a]Lando Summer Undergraduate Research Fellow, 1981.

[b]Present address: Department of Chemistry, Columbia University, New York, NY 10027.

[c]Present address: Materials and Molecular Research Division, Lawrence Berkeley Laboratory, University of California, Berkeley, California 94720

This work was supported by the Office of Energy Research, Chemical Sciences Division of the U.S. Department of Energy under Contract No. DE-AC03-76SF00098; and by the National Science Foundation under Grant No. CHE80-25232.

Abstract

We calculate *ab initio* interaction potentials for electron-methane scattering and use them to perform converged scattering calculations for the electronically and vibrationally elastic rotational-state-to-rotational-state cross sections at 10 eV impact energy. The effective potential has static, local exchange, and polarization terms calculated from extended-basis-set Hartree-Fock wavefunctions for both unperturbed and polarized methane molecules. The polarization potential includes nonadiabatic effects in the semiclassical local-kinetic-energy approximation, and for comparison we also perform calculations based on the adiabatic polarization potential. Five to twelve terms are retained in the angular expansion of the various parts of the interaction potential, and the coupled channels claculations involved 41 total angular momenta, with 1-33 coupled channels for each. The resulting rotationally summed integral cross sections are in excellent agreement with recent experiments for scattering angles 40° and larger, but are larger than experiment at small scattering angles. The rotationally inelastic cross sections for the full potential are smaller than those for the adiabatic potential by about a factor of two.

I. INTRODUCTION

Most quantum mechanical calculations of electron-molecule scattering have been for linear molecules. In that case there are important simplifications in the calculation of the target wavefunction and effective interaction potential and in the solution of the scattering equations.[1] Burke et al.[2] have developed a formalism for treating electron scattering by general polyatomic molecules in the fixed-nuclei approximation. The scattering amplitudes of this method may be used to calculate state-to-state cross sections in the vibrational-rotational sudden approximation, which is expected to be a good approximation for non-dipole cases except near thresholds. In this article we present a laboratory-frame calculation for electron scattering by a nonlinear molecule, namely methane. This has the advantage of yielding state-to-state cross sections directly. We make the rigid-rotator approximation and calculate differential and integral cross sections for pure elastic scattering and for state-to-state rotational excitation processes. We use a general formalism that takes full advantage of the T_d symmetry of the rigid methane molecule. The calculations are carried out for an impact energy of 10 eV. This energy is at the border of the low- and intermediate-energy regions; as far as computational difficulty this energy involves a compromise between the simplification of the rapid convergence of the sum over orbital angular momentum contributions at low energy and the greater validity at intermediate and high energy of local approximations[3] for the electron-target exchange interactions. The border of low- and intermediate-energy is also a crucial one for testing approximations in the treatment of charge polarization (see next paragraph), and it allows for comparison to the experimental differential cross section measurements of Rohr,[4] Tanaka and coworkers,[5] and Newell et al.[6] and to the model potential calculations performed by Gianturco

and Thompson[7,8] using a simple model potential and the formalism of Burke et al.[2,9]

Although it has been demonstrated in previous work that nonempirical scattering calculations based on neglect-of-differential-overlap molecular orbital theory, local exchange approximations, and minimum-basis-set polarization potentials can yield useful accuracy for e^--N_2, e^--CO, e^--C_2H_2, and e^--CO_2 scattering at 10 eV and above,[10] it is also of interest to explore more ab initio treatments. In the present paper we again use local exchange approximations, but we calculate the static potential and the target density for the exchange potential by extended-basis-set Hartree-Fock calculations. Furthermore we approximate the effect of charge polarization in two different ways: by an ab initio extended-basis-set adiabatic polarization potential V^{Pa} and also by the local-kinetic energy semiclassical polarization potential V^{Plke}. The latter is an approximation[11] to the true polarization potential, defined as the difference between the real part of the exact optical potential and the static-exchange potential. V^{Plke} is computationally convenient because it can be calculated from the ab initio static and adiabatic polarization potentials, and hence it provides a way to modify V^{Pa} to account for nonadiabatic effects.

II. SCATTERING THEORY

In this section we present a laboratory-frame formalism for scattering of a structureless particle by a spherical top molecule with T_d symmetry. It is very similar to the formalism used by Secrest and coworkers[12] for Ar-CH_4 scattering; however their formalism only took advantage of the T subgroup of T_d. Furthermore we present our formalism in a general way so that it is reasonably clear how to modify it to treat the scattering of structureless particles by other nonlinear molecules having different symmetry point groups.

The total wavefunction of definite total angular momentum J and projection M on the laboratory z-axis is expressed as

$$\Psi^{JM}(\vec{r},\vec{G}) = \sum_{j=0}^{\infty} \sum_{\alpha=1}^{\alpha_{max}(j)} \sum_{\ell=|J-j|}^{J+j} r^{-1} f^{J}_{j\alpha\ell}(r)\, \mathcal{Y}^{JM}_{j\alpha\ell}(\hat{r},\vec{G}) \qquad (1)$$

In practice, the close coupling approximation cuts off the sum over j at some finite j_{max} which is a decreasing function of J. The vector $\vec{G}$ specifies the orientation (α,β,γ) of the molecule with respect to the laboratory-frame axes, r is the distance from the center of mass of the rotor to the scattering electron, and $\hat{r}$ specifies the angular position (θ,ϕ) of the incident electron, again with respect to laboratory-frame axes. The expansion coefficients $f^{J}_{j\alpha\ell}(r)$ are the scattering particle radial wavefunctions. The total-angular-momentum eigenfunction $\mathcal{Y}^{JM}_{j\alpha\ell}$, where j is the rotational quantum number, α specifies a particular member of the degenerate set for a given j, and ℓ specifies the orbital angular momentum of the scattering particle, is defined in terms of rotor and projectile angular functions as

$$\mathcal{Y}^{JM}_{j\alpha\ell}(\hat{r},\vec{G}) = \sum_{m_\ell=-\ell}^{\ell} \sum_{m_j=-j}^{j} (\ell m_\ell j m_j | JM)\, \psi_{j\alpha m_j}(\alpha,\beta,\gamma)\, Y_\ell^{m_\ell}(\theta,\phi) \qquad (2)$$

where $(\ell m_\ell j m_j | JM)$ is a Clebsch-Gordan coefficient. (All angular momentum coupling coefficients are defined as in Edmonds.[13]) $\psi_{j\alpha m_j}(\alpha,\beta,\gamma)$ is a rotor wavefunction. The rotor wavefunctions for spherical tops are the rotation matrices[13] $D^j_{m_j k}(\alpha,\beta,\gamma)$ for the finite rotations specified by the Euler angles α, β, and γ, which are collectively denoted as $\vec{G}$. In the rotor function m_j is the projection of j on the laboratory z axis, and k is its projection on the rotor z-axis. The spherical top rotor states have a degeneracy of $(2j+1)^2$, i.e.,

$$H_{rotor}(\alpha,\beta,\gamma)\, D^j_{m_j k}(\alpha,\beta,\gamma) = Bj(j+1)\, D^j_{m_j k}(\alpha,\beta,\gamma) \qquad (3)$$

for $-j \le k \le j$ and $-j \le m_j \le j$, where B is the rotational constant; thus we may take any convenient linear combinations as our basis functions. We choose linear combinations that transform as the irreducible representations of the T_d point group, i.e.,

$$\psi^{p\mu}_{jhm_j}(\alpha,\beta,\gamma) = A^{p\mu}_{jhm_j} \sum_{k=-j}^{j} b^{p\mu}_{jhk}\, D^j_{m_j k}(\alpha,\beta,\gamma) \qquad (4)$$

where $A^{p\mu}_{jhm_j}$ is a normalization constant, p specifies the symmetry (A_1, A_2, E, T_1, or T_2), μ specifies the component of the representation (μ = 1 for A_1 and A_2, 1 or 2 for E, and 1, 2, or 3 for T_1 and T_2), and h specifies the h-th basis function of rotational quantum number j for a given p and μ. Now the sum over α in (1) becomes a sum over p, μ, and h.

We will require the matrix elements of the interaction potential between total-angular-momentum eigenfunctions:

$$V^J_{j\alpha\ell j'\alpha'\ell'}(r) = \int d\hat{r} \int d\vec{G}\, \mathcal{Y}^{JM*}_{j\alpha\ell}(\hat{r},\vec{G})\, V(\vec{r},\vec{G})\, \mathcal{Y}^{JM}_{j'\alpha'\ell'}(\hat{r},\vec{G}) \qquad (5)$$

The interaction potential may be written as

$$V(\vec{r},\vec{G}) = \sum_{\lambda=0}^{\infty} \sum_{i=1}^{i_{max}(\lambda)} V_{\lambda i}(r)\, T_{\lambda i}(\theta,\phi,\alpha,\beta,\gamma) \tag{6}$$

where $i_{max}(\lambda)$ is the number of A_1 basis functions with λ nodes in the θ variable, and

$$T_{\lambda i}(\theta,\phi,\alpha,\beta,\gamma) = \zeta_\lambda \sum_{s=-\lambda}^{\lambda} \sum_{q=-\lambda}^{\lambda} a_{iq}^{\lambda}\, D_{sq}^{\lambda *}(\alpha,\beta,\gamma)\, Y_\lambda^s(\theta,\phi) \tag{7}$$

where ζ_λ is a phase factor chosen as

$$\zeta_\lambda = \begin{cases} +1 & \text{even } \lambda \\ -i & \text{odd } \lambda \end{cases} \tag{8}$$

so that $V_{\lambda i}(r)$ is always real, and a_{iq}^{λ} is chosen so that $T_{\lambda i}(\theta,\phi,\alpha,\beta,\gamma)$ transforms under the symmetry operators of the T_d point group according to the A_1 irreducible representation. Thus, for any θ,ϕ, if $\hat{S}$ reorients the rotor (i.e., $\vec{G}$) according to a symmetry operation of T_d, then

$$\hat{S}\, T_{\lambda i}(\theta,\phi,\alpha,\beta,\gamma) = (+1) T_{\lambda i}(\theta,\phi,\alpha,\beta,\gamma) \tag{9}$$

Of course one can also hold the rotor fixed at $\alpha = \beta = \gamma = 0$, for which $D_{sq}^{\lambda}(0,0,0) = \delta_{sq}$, and reorient the scattering particle (i.e., θ,ϕ). Equation (9) holds for this kind of symmetry operation too. The latter interpretation provides a more convenient method for deriving the coefficients a_{iq}^{λ}, and they have been derived by Altmann and Cracknell[14] in this way. Their choice of axes corresponds to reflections in the xy, xz, and yz planes all being symmetry operators; to be consistent with this we let $\alpha = \beta = \gamma = 0$ correspond to $x_H = y_H = z_H < 0$ when x_H, y_H, and z_H are the cartesian coordinate of one of the hydrogen atoms. For this choice the required coefficients can be

obtained from the following expression

$$a^{\ell}_{gm} = \begin{cases} \bar{a}^{\ell}_{m} & m = 0 \\ \bar{a}^{\ell}_{m}/\sqrt{2} & m \neq 0 \end{cases} \tag{10}$$

where $\bar{a}^{\ell}_{m}$ is the quantity tabulated by Altmann and Cracknell for the g-th component for a given ℓ of the A_1 representation. Note there is a sign error in $\bar{a}^{11}_{2}$ in their Table I(a); the correct value is -0.66536331.

Substituting (2), (4), (6), and (7) into (5) yields

$$V^{J}_{j\alpha\ell j'\alpha'\ell'}(r) = \sum_{m_\ell} \sum_{m_j} \sum_{m_{\ell'}} \sum_{m_{j'}} \sum_{\lambda} \sum_{i} \sum_{s} (\ell m_\ell j m_j | JM)(\ell' m_{\ell'} j m_{j'} | JM) V_{\lambda i}(r)\, \zeta_\lambda$$
$$\times \int d\hat{r}\; Y^{m_\ell *}_{\ell}(\hat{r})\; Y^{s}_{\lambda}(\hat{r})\; Y^{m_{\ell'}}_{\ell'}(\hat{r}) \int d\vec{G}\; \psi^{p\mu *}_{jhm_j}(\vec{G})$$
$$\left[\sum_{q=-\lambda}^{\lambda} a^{\lambda}_{iq}\, D^{\lambda *}_{sq}(\vec{G}) \right] \psi^{p'\mu'}_{j'h'm_{j'}}(\vec{G}) \tag{11}$$

According to the discussion above [first interpretation of $\hat{S}$ in eq. (9)], the quantity in brackets has A_1 symmetry; therefore[15] the integral over $\vec{G}$ is proportional to $\delta_{pp'}\delta_{\mu\mu'}$. Thus the problem is block diagonal in p and μ.

We restrict our attention in the rest of this paper to the case where the rotor is initially in the ground rotational state. This state is non-degenerate with A_1 symmetry, hence we can rigorously restrict our basis set to rotor functions with A_1 symmetry. For convenience, for A_1 basis functions, we rewrite (4) in the normalized form

$$\psi_{jhm_j}(\alpha,\beta,\gamma) = N_j\, e^{ik_{max}(j,h)\pi/4} \sum_{k=-k_{max}(j,h)}^{k_{max}(j,h)} a^{j}_{hk}\, D^{j}_{m_j k}(\alpha,\beta,\gamma) \tag{12}$$

where

$$N_j = [(2j+1)/8\pi^2]^{\frac{1}{2}} \tag{13}$$

where $k_{max}(j,h)$ is the highest value of k for which a^j_{hk} is nonzero. Using basis function (12), the matrix element (11) becomes

$$V^J_{jh\ell j'h'\ell'}(r) = N_j N_{j'} \exp[i(k'_{max} - k_{max})\pi/4] \sum_{m_\ell} \sum_{m_j} \sum_{m_{\ell'}} \sum_{m_{j'}} \sum_{\ell} \sum_{i} \sum_{s} \sum_{k} \sum_{k'} \sum_{q}$$

$$\zeta_\lambda \, a^\lambda_{iq} \, a^j_{hk} \, a^{j'}_{h'k'} \, V_{\lambda i}(r) (\ell m_\ell j m_j | JM) (\ell' m_{\ell'}, j' m_{j'} | JM)$$

$$\int d\hat{r} \, Y^{m_\ell *}_\ell(\hat{r}) \, Y^s_\lambda(\hat{r}) \, Y^{m'}_{\ell'}(\hat{r}) \int d\vec{G} \, D^{j*}_{m_j k}(\vec{G}) \, D^{\lambda *}_{sq}(\vec{G}) \, D^{j'}_{m_{j'} k}(\vec{G}) \qquad (14)$$

The integral over $\hat{r}$ can be done in terms of 3j symbols using equations (2.5.6) and (4.6.3) of Edmonds,[13] and the integral over $\vec{G}$ can be done in terms of 3j symbols using his equations (4.2.7) and (4.6.2). This yields

$$V^J_{jh\ell j'h'\ell'}(r) = N_j \text{---} \sum_q 8\pi^2 [(2\ell+1)(2\ell'+1)(2\lambda+1)/4\pi]^{\frac{1}{2}}$$

$$\times \zeta_\lambda \, V_{\lambda i}(r) \, a^\lambda_{iq} \, a^j_{hk} \, a^{j'}_{h'k'} (\ell m_\ell j m_j | JM) (\ell' m_{\ell'}, j' m_{j'} | JM)$$

$$\times (-1)^{m_\ell + m_j - s - k - q} \begin{pmatrix} \ell & \lambda & \ell' \\ 0 & 0 & 0 \end{pmatrix} \begin{pmatrix} \ell & \lambda & \ell' \\ -m_\ell & s & m'_\ell \end{pmatrix}$$

$$\times \begin{pmatrix} j & \lambda & j' \\ -m_j & -s & m_{j'} \end{pmatrix} \begin{pmatrix} j & \lambda & j' \\ -k & -q & k' \end{pmatrix} \qquad (15)$$

where the --- denotes that the beginning of the right-hand side is the same as in the previous equation. This expansion may be further simplified by introducing a 6j symbol as defined in eq. (6.1.5) of Edmonds, i.e.,

$$V^J_{jh\ell j'h'\ell'}(r) = (-1)^{J+\ell+\ell'}\ 8\pi^2 N_j N'_j\ \exp[i(k'_{max} - k_{max})\pi/4]$$

$$\times\ [(2\ell+1)(2\ell'+1)/4\pi]^{\frac{1}{2}} \sum_\lambda \zeta_\lambda (2\lambda+1)^{\frac{1}{2}}$$

$$\times \begin{pmatrix} \ell & \lambda & \ell' \\ 0 & 0 & 0 \end{pmatrix} \begin{Bmatrix} j & \ell & J \\ \ell' & j' & \lambda \end{Bmatrix} \sum_i V_{\lambda i}(r)$$

$$\times \sum_k (-1)^{-k} a^j_{hk} \sum_{k'} a^{j'}_{h'k'} \sum_q (-1)^{-q} a^\lambda_{iq}$$

$$\times \begin{pmatrix} j & \lambda & j' \\ -k & -q & k' \end{pmatrix} \qquad (16)$$

This expression simplifies for $\lambda = 0$, hence it can be rewritten in the following convenient form

$$V^J_{jh\ell j'h'\ell'}(r) = \delta_{jj'}\,\delta_{hh'}\,\delta_{\ell\ell'}(4\pi)^{-\frac{1}{2}} V_{01}(r)$$

$$+ \sum_{\lambda>0} \sum_i B^J_{jh\ell j'h'\ell';\lambda i}\, V_{\lambda i}(r) \qquad (17)$$

where

$$B^J_{jh\ell j'h'\ell';\lambda i} = (-1)^{J+\lambda}\ \exp[i(k'_{max} - k_{max})\pi/4][(2\ell+1)(2\ell'+1)$$

$$\times\ (2\lambda+1)(2j+1)(2j'+1)/4\pi]^{\frac{1}{2}} \zeta_\lambda$$

$$\times \begin{pmatrix} \ell & \ell' & \lambda \\ 0 & 0 & 0 \end{pmatrix} \begin{Bmatrix} j & \ell & J \\ \ell' & j' & \lambda \end{Bmatrix} \sum_k (-1)^{-k} a^j_{hk}$$

$$\times \sum_{k'} a^{j'}_{h'k'} \sum_q (-1)^{-q} a^\lambda_{iq} \begin{pmatrix} j & \lambda & j' \\ -k & -q & k' \end{pmatrix} \qquad (18)$$

in which we replaced N_j and N'_j by their corresponding expressions and permuted the 3j symbol $\begin{pmatrix} \ell & \lambda & \ell' \\ 0 & 0 & 0 \end{pmatrix}$ to $\begin{pmatrix} \ell & \ell' & \lambda \\ 0 & 0 & 0 \end{pmatrix}$. The selection rules associated

with the 3j symbols in eq. (18) restrict the number of nonzero matrix elements as follows:

$$\max(|j'-j|,|\ell'-\ell|) \leq \lambda \leq \min(j'+j,\ell'+\ell) \tag{19}$$

$$\ell + \ell' + \lambda = \text{even} \tag{20}$$

and

$$k' - k - q = 0 \tag{21}$$

The potential matrix is symmetric and real. Its reality is ensured by the proper phase factor chosen above, namely $\zeta_\lambda \exp[i(k'_{max} - k_{max})\pi/4]$. Notice that according to the conventions adopted here the spherical average of the potential becomes $V_{01}(r)/(4\pi)^{\frac{1}{2}}$, not $V_{01}(r)$.

Substituting equations (1)-(3) and (12) into the complete Schrödinger equation and requiring

$$\int d\hat{r} \int d\vec{G}\, Y^{JM*}_{j'h'\ell'}(\hat{r},\vec{G})\,(H-E)\,\Psi^{JM}(\vec{r},\vec{G}) = 0 \tag{23}$$

yields the close coupling equations

$$[-\frac{\hbar^2}{2m}\frac{d^2}{dr^2} + V^J_{jh\ell jh\ell}(r) - \frac{\hbar^2 k_j^2}{2m}]f^J_{jh\ell}(r) = \sum_{j'h'\ell'} V^J_{jh\ell j'h'\ell'}(r)\, f^J_{j'h'\ell'}(r) \tag{24}$$

where

$$k_j^2 = (2m/\hbar^2)[E - Bj(j+1)] \tag{25}$$

and E is the total energy. These equations are to be solved subject to the usual scattering boundary conditions to yield the transition matrix elements $T^J_{jh\ell j'h'\ell'}$. From these the differential and integral cross sections $d\sigma_{jj'}/d\Omega$ and $\sigma_{jj'}$ may be calculated by the formulas of Blatt and Biedenharn[16,17] and the momentum transfer cross sections may be calculated by

$$\sigma^m_{jj'} = 2\pi \int_0^\pi d\theta \sin\theta(1-\cos\theta)\, d\sigma_{jj'}/d\Omega \tag{26}$$

To the extent that the interaction potential for the rigid rotator approximates that for the vibrationally averaged rotor the electronically and vibrationally elastic total cross sections may be obtained by summing over j' for $j = 0$. The resulting cross sections will be called the vibrationally elastic cross sections and labelled $d\sigma_0/d\Omega$, σ_0, and σ_0^m.

The restriction to A_1 symmetry states greatly reduces the number of channels that couple to the ground state. The number of channels that must be considered is further reduced by parity. The parity of a channel state defined by (2) and (12) is $(-1)^{j+\ell}$. The parity of the ground-state channel is thus $(-1)^J$. The resulting savings are summarized in Table I. For typical low-j values the number of channels that must be considered is $(j+1)$, as compared to the degeneracy of $(2j+1)^2$ for a given j if neither symmetry nor parity is considered. The last column of Table I is actually the maximum number of channels that must be considered and applies in the large-J limit. At low J the number of channel functions is further restricted by the triangle inequality

$$|J - j| \leq \ell \leq J + j \tag{27}$$

We would like to emphasize the enormous savings that are achieved by considering both symmetry and parity conservation, as compared to the case when only parity is considered. For example, for $J = 3$, the number of channels for $j_{max} = 11$ is reduced from 562 when only parity is considered to 33 when the full symmetry of CH_4 is considered. This reduction in the number of channels corresponds to a savings of a factor of about 5×10^3 in computer time.

III. CALCULATION OF THE INTERACTION POTENTIAL

For all calculations the C-H bond distance is fixed at 2.0441 a_0, which is the optimum value at the Hartree-Fock level for the basis set of Scanlon et al.[18]

The present calculations were performed using an extended basis set including polarization functions and diffuse functions. This basis set was chosen by analogy to the nitrogen and water molecules, for which we had previously made extensive comparisons of polarization potentials and polarizabilities calculated with various basis sets. The basis chosen for CH_4 is denoted (12,8,3/8,3)/[9,7,3/7,3] in the usual notation. This basis was obtained by starting with the Huzinaga (11,7) carbon basis[19] and contracting the first four s functions with the atomic 1s coefficients and the first two p functions with the sp coefficients. Diffuse s and p functions were added by geometric expansion. Valence 3d polarization functions were added with exponential parameters (1.5,0.35) taken from van Duijneveldt,[20] and another polarization function was added with an exponential parameter (0.08) optimized for the polarizability of methane by Werner and Meyer.[21] For hydrogen we used Huzinaga's[22] seven s functions with the first two contracted plus a diffuse s function obtained by geometric expansion. Three p functions with exponential parameters 1.8, 0.6, and 0.2 were also added. The value 0.2 is taken from Werner and Meyer[21] and the other functions have parameters differing by factors of 3 and 9. Putting these functions together yields 122 primitives and 112 contracted functions, which are combined into canonical orthonormal orbitals. To avoid linear dependency, only 111 of the canonical orthonormal orbitals are kept for the final calculations.

The wavefunctions, all the polarization potentials, and many of the static potentials were calculated on a CDC 7600 computer using the program MDHONDO.[23] The rest of the static potentials were calculated on a VAX computer using a slightly modified version of the NYU gaussian properties program.[24]

The static and adiabatic polarized potentials $V^S(\vec{r},\vec{G})$ and $V^{SPa}(\vec{r},\vec{G})$ are defined elsewhere.[25] In particular they represent the interaction of a negative test charge with the unperturbed and fully relaxed target charge clouds, respectively.

The adiabatic polarization potential is then defined by

$$V^{Pa}(\vec{r},\vec{G}) = V^{SPa}(\vec{r},\vec{G}) - V^S(\vec{r},\vec{G}) \tag{28}$$

The energy-dependent exchange potential $V^E(\vec{r},\vec{G},E)$ was calculated from the static target density by the semiclassical exchange approximation[3]

$$V^E(\vec{r},\vec{G},E) = \tfrac{1}{2}[E - V^S(\vec{r},\vec{G})] - \tfrac{1}{2}\{[E - V^S(\vec{r},\vec{G})]^2 + 4\pi\rho(\vec{r},\vec{G})\}^{\frac{1}{2}} \tag{29}$$

where $\rho(\vec{r},\vec{G})$ is the electronic charge density of the unperturbed target.

The adiabatic model overestimates the polarization effect, even at low impact energies, because the scattering electron is speeded up by the field of the target and the target polarization does not have enough time to respond fully to the scattered charge. We attempt to account for this effect by the local-kinetic-energy semiclassical polarization model presented elsewhere.[11] In this model the polarization potential is

$$V^{Plke}(\vec{r},\vec{G},E) = [1 - T_{loc}(\vec{r},\vec{G})/\Delta]^{-1}\, V^{Pa}(\vec{r},\vec{G}) \tag{30}$$

where Δ is the effective excitation energy, $T_{loc}(\vec{r},\vec{G})$ is the local kinetic energy

$$T_{loc}(\vec{r},\vec{G}) = E - V^{SE}(\vec{r},\vec{G},E) \tag{31}$$

and $V^{SE}(\vec{r},\vec{G},E)$ is the static-exchange potential

$$V^{SE}(\vec{r},\vec{G},E) = V^{S}(\vec{r},\vec{G}) + V^{E}(\vec{r},\vec{G},E) \tag{32}$$

The total potential used in the scattering calculations is the sum of $V^{SE}(\vec{r},\vec{G},E)$ and either $V^{Pa}(\vec{r},\vec{G})$ or $V^{Plke}(\vec{r},\vec{G},E)$.

The effective excitation energy is most readily evaluated by the method used by Slater and Kirkwood[26] for approximating the dispersion interaction between two atoms or molecules. This yields[27,28]

$$\Delta = (N_{val}/\alpha_d)^{\frac{1}{2}} \tag{33}$$

where N_{val} is the number of electrons in the outer shell of the molecule and α_d is the static dipole polarizability. Using $N_{val} = 8$ and the most accurate available value[28] for α_d yields $\Delta = 18.52$ eV, which is somewhat higher than the ionization potential (12.98 eV).[29]

The actual orientation $(\vec{r},\vec{G})$ at which the potentials were calculated are most conveniently specified in relative coordinates (χ,ϕ_χ). These are values of (θ,ϕ) when $\vec{G}$ is chosen to put one C-H bond on the positive z axis. Then the region to be covered by actual calculations is $0 \le \chi \le 4\tau$ and $0 \le \phi_\chi \le 60°$. Here τ is one eighth the HCH bond angle and equals 13.68°. Values of χ and ϕ_χ outside the region all correspond by symmetry to a value within the region. The static and exchange potentials were calculated for twelve different orientations (χ,ϕ_χ) = (0,0), (2τ,0), (2τ,60), (4τ,0), (4τ,60), (0.5τ,30), (τ,30), (2τ,30), (3τ,0), (3τ,30), (3τ,60), and (4τ,30) for each of 26 values of r in the range 0.1-6.4 a_0 and for the first five of these orientations for each of three values of r in the range 10-30 a_0. Additional calculations at (τ,0) and (τ,60) were carried out for r = 1.0-3.1 a_0.

The adiabatic polarization potential was calculated for the first five orientations for each of 19 values of r in the range 0.1-30 a_0. These values are used to generate a combined analytic and spline representation of the full potentials (SEPa and SEP1ke) for all $(\vec{r},\vec{G})$ as described in the next section.

At large r the adiabatic polarization potential has the asymptotic form

$$V^{Pa}(\vec{r},\vec{G}) \underset{r\to\infty}{\sim} \alpha_d/(2r^4)$$

Using the calculated values at $r = 30\ a_0$ yields $\alpha_d = 15.9\ a_0^3$, which may be compared to the accurate value[28] of $17.27\ a_0^3$. The difference of 8% is probably due mainly to correlation effects.

IV. FITTING THE POTENTIAL

For computational purposes we write the potential in three parts

$$V^{SEP}(\vec{r},\vec{G},E) = V^{en}(\vec{r},\vec{G}) + V^{eeE}(\vec{r},\vec{G}) + V^{P}(\vec{r},\vec{G},E) \tag{34}$$

where

$$V^{eeE}(\vec{r},\vec{G},E) = V^{ee}(\vec{r},\vec{G}) + V^{E}(\vec{r},\vec{G},E) \tag{35}$$

$V^{ee}(\vec{r},\vec{G})$ and $V^{en}(\vec{r},\vec{G})$ are the electron-electron and electron-nucleus parts of the static potential, and $V^{P}(\vec{r},\vec{G},E)$ denotes either $V^{Pa}(\vec{r},\vec{G})$ or $V^{Plke}(\vec{r},\vec{G},E)$.

The electron-nucleus part of the static potential may be calculated analytically as the sum of five coulomb interactions. If the coordinates of the hydrogen atoms when $\alpha = \beta = \gamma = 0$ are denoted $(R,\theta_{Hk},\phi_{Hk})$, then the expansion of this contribution in symmetrized harmonics is given by

$$V^{en}(\vec{r},\vec{G}) = \sum_{\lambda=0}^{\infty} \sum_{i=1}^{i_{max}(\lambda)} V^{en}_{\lambda i}(r)\, T_{\lambda i}(\theta,\phi,\vec{G}) \tag{36}$$

where

$$V^{en}_{\lambda i}(r) = \begin{cases} -\left(\frac{6}{r} + \frac{4}{r_>}\right)\sqrt{4\pi} & \lambda = 0 \\ -\frac{4\pi}{2\lambda+1}\frac{r_<^{\lambda}}{r_>^{\lambda+1}} \sum_{k=1}^{4} T_{\lambda i}(\theta_{Hk},\phi_{Hk},\vec{G}) & \lambda \neq 0 \end{cases} \tag{37}$$

$$r_< = \min\,(r,R) \tag{38}$$

and

$$r_> = \max\,(r,R) \tag{39}$$

In practice the sum over λ must be truncated at λ_{max}. We found that the sum is very slowly convergent to the sum of the five coulomb interactions, especially for the electron near a hydrogen nucleus. However the addition or deletion of a few higher-λ terms has only a small effect on the scattering. For example the T matrix elements for $J = 0$ differ by only 0.5-2% for

calculations with $\lambda_{max} = 13$ and 11, which correspond to 12 and 9 terms in the expansion respectively. Thus for all production runs we set $\lambda_{max} = 13$.

$V^{eeE}(\vec{r},\vec{G},E)$ was calculated by subtracting the five coulomb interactions from $V^{SE}(\vec{r},\vec{G})$. It was expanded as

$$V^{eeE}(\vec{r},\vec{G},E) = \sum_{\lambda=0}^{\lambda_{max}} \sum_{i=1}^{i_{max}(\lambda)} V_{\lambda i}^{eeE}(r,E)\, T_{\lambda i}(\theta,\phi,\vec{G}) \qquad (40)$$

by retaining N terms on the right side of (40), substituting N values of $V^{eeE}(\vec{r},\vec{G},E)$, and solving the resulting N simultaneous equations for the first N of the $V_{\lambda i}^{ee\lambda}(r,E)$. We tried various sets of N points and found that an optimum set must be chosen carefully for an accurate expansion. For N too small the sum is not well converged; for N too large or for the wrong choice of $(\vec{r},\vec{G})$ values, the $V_{\lambda i}^{eeE}(r,E)$ are inaccurate, presumably because the differences between some of the included $V^{eeE}(\vec{r},\vec{G},E)$ become relatively small and sensitive to small numerical errors. For the final fits we chose $N = 5$ ($\lambda_{max} = 7$) for $r = 0.1$–$1.0\ a_0$ and 3.1–$6.4\ a_0$ and $N = 8$ ($\lambda_{max} = 10$) for $r = 1.3$–$2.8\ a_0$. The $N = 5$ set was $(\chi,\phi_\chi) = (0,0)$, $(2\tau,0)$, $(2\tau,60)$, $(4\tau,0)$, and $(4\tau,60)$, and the $N = 8$ set consisted of these points plus $(3\tau,0)$, $(3\tau,60)$, and $(4\tau,30)$. A measure of the accuracy of the resulting representation was obtained by using the truncated sums of equation (40) to calculate $V^{eeE}(\vec{r},\vec{G},E)$ at points other than the ones used to generate the components $V_{\lambda i}^{eeE}(r,E)$. These checks indicate that the present representation is accurate to 1% or better for $r \leq 1.6\ a_0$ and $r \geq 2.5\ a_0$, with a worst error of less than about 5% occurring for the case where the electron is close to an H.

Each resulting $V_{\lambda i}^{eeE}(r,E)$ for $\lambda = 0$–7 is represented by the analytic form

$$V^{X}_{\lambda i}(r,E) = c^{X}_{\lambda i}\, r^{\lambda} + d^{X}_{\lambda i}\, r^{\lambda+1} \tag{41}$$

with X = eeE for $r \leq 0.1\ a_0$, by a 14-node spline fit[30] for $r = 0.1\text{-}2.044\ a_0$, where there is a cusp, by another 14-node spline fit for $r = 2.044\text{-}7.0\ a_0$, and by

$$V^{eeE}_{01}(r,E) = 10(4\pi)^{\frac{1}{2}}/r + f_{01}(E)/r^2 + g_{01}(E)/r^3 \tag{42}$$

and

$$V^{eeE}_{\lambda i}(r,E) = e_{\lambda i}(E)/r^{\lambda+1} + f_{\lambda i}(E)/r^{\lambda+2} \tag{43}$$

for $r \geq 7.0\ a_0$. The $V^{eeE}_{\lambda}(r,E)$ components with $\lambda = 8\text{-}10$ are set equal to zero for $r \leq 1.0\ a_0$ and $r \geq 3.1\ a_0$; each of these components is represented by a 5-node spline fit for $r = 1.0\text{-}2.044\ a_0$ and by a 6-node spline fit for $r = 2.044\text{-}3.1\ a_0$.

The adiabatic polarization potential was expanded as

$$V^{Pa}(\vec{r},\vec{G}) = \sum_{\lambda=0}^{\lambda_{max}} \sum_{i=1}^{i_{max}(\lambda)} V^{Pa}_{\lambda i}(r)\, T_{\lambda i}(\theta,\phi,\vec{G}) \tag{44}$$

with $\lambda_{max} = 7$. Each component $V^{Pa}_{\lambda i}(r)$ is represented by (41) with X = Pa for $r \leq 0.1\ a_0$, by a 17-node spline fit for $r = 0.1\text{-}7.0\ a_0$, and by

$$V^{Pa}_{01}(r) = -\frac{\alpha_{01} A^{X}_{01}}{2r^4} + \frac{B^{X}_{01}}{r^6} + \frac{C^{X}_{01}}{r^7} \tag{45}$$

and

$$V^{Pa}_{\lambda i}(r) = \frac{A^{X}_{\lambda i}}{r^{\lambda+2}} + \frac{B^{X}_{\lambda i}}{r^{\lambda+4}} \qquad \lambda \neq 0 \tag{46}$$

with X = Pa and $A^{Pa}_{01} = (4\pi)^{\frac{1}{2}}$ for $r \geq 7.0\ a_0$. The parameter α_{01} is the spherically averaged static dipole polarizability. For the fit we used our calculated value of $15.9\ a_0^3$.

Using the above fits to $V^{SE}(\vec{r},\vec{G},E)$ and $V^{Pa}(\vec{r},\vec{G})$ we calculated $V^{Plke}(\vec{r},\vec{G},E)$ at the eight (χ,ϕ_χ) values (0,0), (2τ,0), (2τ,60), (3τ,0), (3τ,60), (4τ,0) (4τ,30), and (4τ,60) and fit it by

$$V^{Plke}(\vec{r},\vec{G},E) = \sum_{\lambda=0}^{\lambda_{max}} \sum_{i=0}^{i_{max}(\lambda)} V_{\lambda i}^{Plke}(r,E)\, T_{\lambda i}(\theta,\phi,\vec{G}) \qquad (47)$$

with $\lambda_{max} = 10$ for all r. The 8-term expansion has much larger relative errors for $V^{Plke}(\vec{r},\vec{G},E)$ near the nuclei than it has for $V^{eeE}(\vec{r},\vec{G},E)$, but these errors are not very important because $V^{SE}(\vec{r},\vec{G},E)$ dominates $V^{Plke}(\vec{r},\vec{G},E)$ there. Checking the values produced by (47) at $(\theta,\phi,\vec{G})$ values not used for the fit indicates that the error in fitting $V^{Plke}(\vec{r},\vec{G},E)$ is at most about 2% of $V^{SE}(\vec{r},\vec{G},E)$.

The components $V_{\lambda i}^{Plke}(r,E)$ were represented by (41) with X = Plke for $r \leq 0.1\ a_0$, by a spline fit with the same nodes as for $V_{\lambda i}^{eeE}(r,E)$ at r = 0.1-7.0 a_0, and by (45)-(46) with X = Plke and $A_{01}^{Plke} = (4\pi)^{\frac{1}{2}}(1+E/\Delta)^{-1}$ at $r \geq 7.0\ a_0$.

Various aspects of the interaction potentials are illustrated in Figures 1-5. Notice that the adiabatic (Pa) and local-kinetic-energy nonadiabatic (Plke) polarization potentials differ substantially for r = 0-4 a_0 for all three directions of approach shown in Figures 1-3; however, the static-exchange part of the effective potential dominates the polarization part at short and intermediate r, so differences between the SEPa and SEPlke are usually less than about 20%. Larger differences occur in the tail region where the polarization potential dominates; in these regions the SEPa effective potential is higher than the SEPlke one by as much as 35%. The λ components of the potentials, Figures 4 and 5, show cusps at the C-H bond distance. The cusp

in the spherical average is not a very significant feature, but it is quite distinct for $\lambda = 3$ and all the higher λ's.

V. NUMERICAL SOLUTION OF THE CLOSE COUPLING EQUATIONS

In order to solve the close coupling equations, the Minnesota Numerov code[31] (MNN, version 80-10A) was used to compute T matrix elements for total angular momenta ranging from $J = 0$ to $J = 40$. Convergence of the numerical solutions was carefully checked for all integration parameters. The starting point of the numerical integration was increased gradually from $R_0 = 10^{-5}\ a_0$ for $J = 0$ to $R_0 = 20\ a_0$ for $J = 40$. The criterion used for large J ($J \geq 11$) was

$$R_0 \approx (\ell_{min}/2)\ a_0$$

where ℓ_{min} is the minimum relative angluar momentum in any of the coupled channels. The ending point of the integration varied from $R_{max} = 30\ a_0$ for $J = 0$ to $R_{max} = 100\ a_0$ for $J = 40$. The first 4 steps were carried out with an optimized initial stepsize of $5 \times 10^{-5}\ a_0$, then the stepsize was controlled by a variable-stepsize algorithm[31] with a parameter DELTA. For $J \leq 10$ the stepsize was allowed to increase according to the algorithm with no constraint, and it grew as large as $0.4\ a_0$ in some cases. For $J \geq 11$, an upper limit of $0.064\ a_0$ had to be enforced to insure good convergence since at large J the solutions become quite sensitive to the accuracy of the large-r integration. The convergence of the solutions relative to the parameter DELTA was monitored for $J = 0$, 1, 3, 13, 20, and 30, and DELTA was chosen for other J by generalizing this experience. A typical converged value was DELTA = -1.5×10^{-8}.

There has been interest recently in comparing the performance of various numerical integration schemes for the solution of coupled channel scattering equations. The hybrid variable-interval variable stepsize VIVAS[32] has been judged by Thomas *et al.*[33] to be the most generally efficient code. We made a careful comparison of the efficiency of our Numerov code to that of the

VIVAS code[34] (our version 82-2) for the present problem. We carefully optimized both codes to obtain the most efficient integrations consistent with 1% accuracy in the first row of the T matrix. Both codes were optimized with respect to initial and maximum stepsizes and the starting and ending points of the integration. MNN was also optimized with respect to DELTA; VIVAS was also optimized with respect to the switchover from the log derivative (LODG) method[35] at small r to the variable-interval variable-step (VIVS) method[36] at large r, with respect to the number of steps per interval in VIVS, and with respect to the parameter TOFF that controls the stepsize at which perturbation corrections of the wavefunction and its derivatives are made in VIVS. The parameters were optimized for a 2-channel J = 0 run and then re-optimized for a 4-channel J = 30 run. The optimized parameters for J = 0 were also used for a 10-channel run and the resulting T matrix elements in the first row still agreed to 1%. The computation times for these runs are shown in Table II. We conclude that the efficiencies of the two codes are the same within a factor of about 1.7; this is consistent with the conclusion reached by Thomas *et al.*[33] for an electron-N_2 test case.[37] Since the MNN code has less parameters to optimize we found it to be more convenient, and we used MNN for the production runs.

VI. RESULTS

The rotational close coupling calculations were carried out using the laboratory-frame formalism of section II. In this scheme, a basis set of rotational-orbital quantum numbers is determined by specifying a maximum total angular momentum J_{max} and for every J a maximum rotational quantum number j_{max}. The centrifugal sudden decoupling index n defined by[38]

$$n = \ell - \max \begin{Bmatrix} |J-j| \\ J \end{Bmatrix} \tag{48}$$

was assigned a maximum value $n_{max} = 2$ for $J \geq 4$, but for $J = 0\text{-}3$ it was not restricted beyond the limitations imposed by j_{max}. Convergence with respect to n_{max} was checked at $J = 3$ and $j_{max} = 11$ and at $J = 10$ with $j_{max} = 7$. The first row T matrix elements changed by only 0.5-2.0% as n_{max} was changed from 2 to 3 and by 1.0-3.0% as n_{max} was changed from 2 to ∞, with the least errors made in the largest elements. Thus the limitation on n_{max} causes negligible truncation error in these tests. These tests are actually more strict than required for our procedure since we always converge with respect to j_{max} at a given n_{max}.

In order to illustrate the overall degree of convergence relative to J_{max}, j_{max}, and the number of channels N, results for the SEPa potential will be presented for three basis sets (to be called I, II, and III). The maximum rotational angular momentum quantum numbers j_{max}, the number of channels N, and the CPU time on the VAX 11/780 computer are tabulated for each total angular momentum J or range of J. The criterion for constructing basis III was that the larger first-row T matrix elements are converged to 1% or better and that relative errors in less important first-row elements do not exceed 3%. The other bases are used only for demonstrating convergence.

Assuming that the molecule is initially in its electronic and rotational ground state, the first-row T matrix elements obtained from the numerical solution of the coupled differential equations were used to compute state-to-state rotationally elastic and inelastic integral cross sections $\sigma_{0j'}$, momentum transfer cross sections $\sigma^m_{0j'}$, and differential cross sections $\frac{d\sigma_{0j'}}{d\Omega}(\theta)$. These cross sections were summed over j' ($j' = 0$-11) to obtain the (electronically and vibrationally elastic) rotationally summed cross sections σ_0, σ^m_0, and $\frac{d\sigma_0}{d\Omega}(\theta)$, respectively.

State-to-state and vibrationally elastic differential cross sections obtained using the 3 bases of Table III are given in Table IV for the SEPa potential and all three scattering bases at 4 scattering angles, and in Tables V and VI for the SEPa and SEP1ke potentials and basis III at 21 scattering angles. Basis III is our largest and consequently most converged basis set. The SEPa and SEP1ke rotationally elastic ($j = 0$, $0 \rightarrow 0$) and the largest rotationally inelastic ($0 \rightarrow j'$) differential cross sections are compared in Figure 6; while the rotationally summed differential cross sections are compared in Figure 7 to each other, to experiment,[4-6] and to other theoretical results.[8]

In Table VII, the SEPa integral and momentum transfer cross sections obtained using the 3 bases are compared to one another and to the corresponding SEP1ke cross sections obtained with basis III. Table VIII gives the partial wave contributions q_ℓ to the integral state-to-state and rotationally summed cross sections. Elastic and momentum transfer cross sections are compared to experiment[5,39,40] and to other theories[7,41] in Table IX. Finally, in Table X we compare the various experimental[5,6] and theoretical[8] values of the ratio of $\frac{d\sigma_0}{d\Omega}(\theta)$ to $\frac{d\sigma_0}{d\Omega}(\theta' \neq 0)$; our own results in this table are for basis III.

The two previous theoretical studies to which we compare are those of Buckingham et al.[41] and Gianturco and Thompson.[8,9] Buckingham et al. made a spherical average of the proton field to CH_4 to obtain central-field SCF orbitals. They then calculated the integral cross section by phase shifts for the resulting static potential. The Gianturco-Thompson calculation is more in the spirit of the present results. However it is less complete in several ways. Instead of an exchange potential they used an orthogonalization procedure. Instead of an ab initio polarization potential they used the spherical approximation given by

$$V^P(r) = -(\alpha/2r^4)\{1 - \exp[-(r/r_0)]\}^6 \qquad (49)$$

Both the form of (49) and the parameter r_0 were chosen by comparison of the scattering results to experiment. In the expansion of the static potential they used 5 terms as compared to 8 or 12 terms for parts of the present potential. They used a body-frame treatment of the scattering involving four symmetries with 5 coupled channels each. A converged body-frame treatment, which would be equivalent to a converged space-frame treatment such as employed here, would involve five symmetries and more coupled channels per symmetry.

VII. DISCUSSION AND COMPARISON TO EXPERIMENT

Tables IV and VII show that the rotationally summed SEPa differential, integral, and momentum transfer cross sections are converged to better than 1.5% in most cases. The convergence of the state-to-state integral cross sections for $j' \geq 7$ and the state-to-state differential cross sections for $j' \geq 3$ is not as good, but we note that the worse relative errors occur in comparatively small state-to-state cross sections, and the convergence of the important cross sections is acceptable. We also note that the $j = 0 \rightarrow j' = 10$ or 11 cross sections were of negligible mangitude and poorly converged, hence we chose not to report them in any of Tables IV-VIII.

As discussed at the end of section IV, the differences between the SEPa and SEP1ke effective potentials are not large. Nevertheless, the scattering is quite sensitive to the choice of potential, especially for low total angular momenta ($J = 0$-3). This is most clear in the partial cross sections of Table VIII and in the changes in the cross sections of Gianturco and Thompson when their empirical parameter is changed by only 0.04 a_0; these changes are illustrated in Table X. Tables V-VIII and Figures 6 and 7 all illustrate that the rotationally summed cross sections are less sensitive to the choice of potential than are the individual state-to-state cross sections. The nonadiabatic SEP1ke potential is the theoretically best justified one, and the results for the SEPa potential are presented only for reference and to test how important the nonadiabatic corrections are. It is encouraging therefore that Figure 7 shows the SEP1ke results to be in excellent agreement with the experimental rotationally summed differential cross sections. This agreement is also exhibited in the ratios of differential cross sections in Table X. The SEPa results are also in qualitative agreement with experiment, but the agreement is definitely worse than

than for the SEP1ke results. While the rotationally summed cross sections for the two potentials are similar, Tables V-VIII and Figure 6 show that SEPa scattering is much less elastic. Both the agreement of rotationally summed cross sections with experiment and the theoretical reasonableness of the model favor the SEP1ke results. Thus the SEP1ke results are the final predicted values of this study, and in particular we believe that the SEP1ke rotationally inelastic cross section of 10.5 a_0^2 is a more reliable prediction than the SEPa rotationally inelastic cross section of 23.3 a_0^2. No experiments that resolve j' are available yet for CH_4.

The proper choice of the potential deserves a further comment. Although it is well established in the literature[42] that the adiabatic polarization potential is too attractive, there have been only a few studies that incorporate nonadiabatic effects in a nonempirical way. Since the target does not have infinite time to respond to the field of the incident electron, and since the time available depends on the local kinetic energy of the incident electron, a realistic local approximation to the polarization potential should be explicitly energy dependent. However the usual practice has been to use energy-independent empirical cutoff parameters to account for nonadiabatic results. Not only is this practice unsatisfactory from a fundamental point of view, but also the scattering results can be very sensitive to the parameter. Table X shows that the ratio of the differential cross section at 60° to its value at 120° computed by Gianturco and Thompson changes by nearly an order of magnitude when the parameter r_0 is changed by 9.5%. In previous work[10] we have successfully used semiempirical minimum-basis-set calculations to compute polarization potentials, and we have obtained good scattering results for a variety of systems at several energies. The

minimum-basis-set restriction in these calculations mimics the nonadiabatic effects by not letting the target completely relax to its minimum energy configuration. The present treatment involves a less empirical procedure for diminishing the adiabatic response of the target, namely the semi-classical local-kinetic-energy approximation derived from a formal expansion of the exact optical potential.[11] As discussed in the previous paragraph, it is gratifying that this ab initio model is so successful.

It is mentioned above that the largest differences between the scattering results for the adiabatic and nonadiabatic potentials are in the s, p, d, and f waves. The last column of Table VIII shows that d-wave scattering dominates for both potentials, contributing 76% for the SEPa potential and 61% for the SEP1ke potential; this accounts for the d-wave dominated shapes of the rotationally summed differential cross sections in Figure 7. Pure d-wave scattering would have local minima at 55° and 125° and a local maximum at 90°. The results for the SEPa potential actually show two local minima and a local maximum, but in the experimental results and SEP1ke results the first local minimum is replaced by a shoulder due to the larger contributions from other partial waves. The SEP1ke results also show a deeper local minimum than the SEPa results at large angles, and again this is in better agreement with the most recent experiments. These shape features of the differential cross sections are summarized in Table X, which shows that our SEP1ke results are within the experimental range for the shape of the differential cross section at 40°-120°. This table also shows the great sensitivity (mentioned above) of the Gianturco-Thompson results to small variations in their empirical parameter. (The value of this parameter used for Figure 7 was chosen to maximize agreement with experiment.) This great

sensitivity of the shape of the rotationally summed differential cross section makes the good agreement of the present nonempirical SEP1ke results even more satisfying.

The comparisons of integral cross sections in Table IX are harder to interpret because the experimental result of Tanaka includes an extrapolated contribution from the small-angle scattering that they did not measure. The error estimate of the integral cross section given by Tanaka et al.[5] and given in Table IX is stated by them to include only the uncertainty due to the precision of their individual measurements of $d\sigma_0/d\Omega$. It does not include the other errors that affect their value of σ_0, in particular the quality of the fit and the extrapolation used to compute σ_0 by integration. Their extrapolation would appear to be particularly sensitive to error in this case because of the large (38%) uncertainty at 10 eV of their differential cross section at the smallest scattering angle (30°) for which they measured it. A further indication of the uncertainty of the 30° measurement is provided by the 30/90 column of Table X; this column shows a large discrepancy between the measurement of Tanaka et al.[5] at 30° and their fit at this angle. The uncertainty in the small-angle experimental differential cross section and in the extrapolation of this cross section to compute the integral cross section explains why the SEP1ke differential cross section agrees bettern with Tanaka et al.'s[5] measurement than the SEP1ke integral cross section agrees with the integral cross section they calculated from their measurements. Nevertheless it is disturbing that the present calculation of the integral cross section also exceeds the recent direct measurement of Barbarito et al. Both Barbarito et al.'s[40] value and Tanaka et al.'s[5] value are considerably lower than the values obtained in the older (1927-1930)

measurements reviewed by Kieffer.[39] The comparison to reference 40 may indicate that the forward peak in the elastic differential cross sections predicted by both potentials studied here is too large.

In summary, we have presented an ab initio calculation of electron-methane cross sections at 10 eV using energy-dependent local potentials. We have used the full molecular symmetry of the target to reduce the number of coupled channels in the scattering calculations. The calculated differential cross sections for the effective potential based on the nonadiabatic semiclassical local-kinetic-energy polarization potential are in good agreement with experimentally measured results for electronically and vibrationally elastic scattering for a wide range of scattering angles (40°-140°). The results are consistent with the importance of nonadiabatic effects even at low energy. It remains an open problem to resolve the apparent discrepancy in the calculated and apparent experimental cross sections for small scattering angles ($\theta \leq 30°$).

VIII. ACKNOWLEDGMENTS

We are grateful to Don Secrest for several discussions of his $Ar-CH_4$ calculations, to Hiroshi Tanaka for sending his experimental results prior to publication, and to Sandor Trajmar for additional assistance in making the comparison to experiment. This work was supported in part by the National Science Foundation under grant no. CHE80-25232, and by the Office of Energy Research, Chemical Sciences Division of the U.S. Department of Energy under Contract No. DE-AC03-76SF00098.

Table I. Decomposition of the rotational basis in T_d symmetry

λ	number of terms in potential (with A_1 symmetry)	j	number of A_1 rotational basis functions	number of channel functions with symmetry A_1 and parity $(-1)^J$
0	1	0	1	1
1,2	0	1,2	0	0
3,4	1	3,4	2j + 1	j + 1
5	0	5	0	0
6-11	1	6-11	2j + 1	j + 1
12	2	12	50	26
13,14	1	13,14	2j + 1	j + 1

Table II. Comparison of efficiences of close coupling codes

J	no. of channels	code	eigenphase sum (mod π)	cpu time (s)[a]
0	2	VIVAS	2.6598	24
		MNN	2.6599	24
0	10	VIVAS	2.9392	75
		MNN	2.9397	126
30	4	VIVAS[b]	6.535×10^{-4}	60
		MNN	6.538×10^{-4}	40

[a]Central processor unit time (in seconds) for execution in double precision on the University of Minnesota Chemistry Department Digital Equipment Corporation VAX 11/780 computer.

[b]In this case the optimum mode of operation of the VIVAS code was to use the VIVS method over the whole region of integration.

Table III. Basis sets for electron-methane scattering

J	Basis I			Basis II			Basis III		
	$j_{max}(J)$	N	CPU (min)	$j_{max}(J)$	N	CPU (min)	$j_{max}(J)$	N	CPU (min)
0	12[a]	10	3.5	12[a]	10	3.5	13[b]	12	11.9
1	11	17	13.5	11	17	13.5	12[a]	19	40.9
2	10	22	26.6	10	22	26.6	11	25	41.4
3	9	25	28.4	10	29	64.3	11	33	66.7
4[c]	9	19	7.4	10	24	15.8	11	28	27.0
5	9	20	8.5	10	22	10.9	11	27	22.0
6	9	24	16.0	9	24	16.0	10	27	22.3
7	8	23	14.1	8	23	14.1	9	27	21.8
8	6	13	3.7	7	18	9.0	8	24	19.7
9	6	13	4.1	7	18	9.8	8	24	20.8
10	6	13	4.1	6	13	4.1	7	18	9.6
11-19	6	13	45.0	6	13	45.0	6	13	45.0
20	4	8	1.9	4	8	1.9	6	13	5.7
21-29	4	8	18.0	4	8	18.0	4	8	18.0
30	0	1	0.4	3	4	0.7	4	8	2.0
31-35	...	0	...	0	1	1.9	3	4	3.3
36-40	...	0	...	...	0	...	0	1	2.0
Total CPU (min)			195			255			380

[a]This includes only the first $j = 12$ basis function, i.e., the one for which b^{pu}_{jhk} is nonzero for $k = 0$.

[b]This includes both $j = 12$ basis functions.

[c]For $J \leq 3$, there is no limit on the centrifugal sudden decoupling index n. For $J \geq 4$, $n_{max} = 2$.

Table IV. State-to-state and vibrationally elastic differential cross sections (a_0^2/sr) at selected scattering angles, using the SEPa potential.

θ (deg)	Basis	$d\sigma_{0j'}/d\Omega$							$\frac{d\sigma_0}{d\Omega}$
		j' = 0	3	4	6	7	8	9	
0	I	4.07(+1)	5.78(-4)	1.04	7.62(-3)	8.15(-6)	6.94(-7)	4.80(-8)	4.17(+1)
	II	4.09(+1)	6.63(-4)	1.04	8.03(-3)	9.43(-6)	7.31(-7)	4.62(-8)	4.19(+1)
	III	4.11(+1)	5.38(-4)	1.04	8.18(-3)	9.18(-6)	8.21(-7)	4.51(-8)	4.22(+1)
60	I	2.26	1.12	1.10	3.50(-3)	3.01(-4)	1.95(-6)	1.57(-7)	4.49
	II	2.25	1.12	1.10	3.70(-3)	3.21(-4)	2.10(-6)	1.68(-7)	4.48
	III	2.26	1.13	1.10	3.77(-3)	3.27(-4)	2.23(-6)	1.54(-7)	4.50
120	I	8.99(-2)	4.04(-1)	1.11	1.30(-2)	4.54(-4)	2.48(-6)	2.34(-7)	1.61
	II	8.70(-2)	4.05(-1)	1.11	1.35(-2)	4.85(-4)	2.60(-6)	2.57(-7)	1.61
	III	9.01(-2)	4.04(-1)	1.11	1.36(-2)	4.94(-4)	2.86(-2)	2.19(-7)	1.62
180	I	1.74(+1)	5.05(-1)	1.55	3.48(-2)	1.34(-3)	4.26(-6)	2.52(-6)	1.95(+1)
	II	1.74(+1)	5.18(-1)	1.55	3.61(-2)	1.40(-3)	4.55(-6)	2.67(-6)	1.95(+1)
	III	1.73(+1)	5.14(-1)	1.55	3.63(-2)	1.43(-3)	4.91(-6)	3.27(-6)	1.94(+1)

Table V. State-to-state and vibrationally elastic differential cross sections (a_0^2/sr) at selected scattering angles, using basis III and the SEPa potential.

θ	$d\sigma_{0j'}/d\Omega$							$\frac{d\sigma_0}{d\Omega}$
(deg)	j' = 0	3	4	6	7	8	9	
0	4.11(+1)	5.38(-4)	1.04	8.18(-3)	9.18(-6)	8.21(-7)	4.51(-8)	4.22(+1)
5	3.69(+1)	1.65(-2)	1.04	8.12(-3)	1.34(-5)	8.16(-7)	4.74(-8)	3.79(+1)
10	3.10(+1)	6.73(-2)	1.045	7.95(-3)	2.59(-5)	8.06(-7)	5.42(-8)	3.21(+1)
15	2.57(+1)	1.49(-1)	1.05	7.68(-3)	4.59(-5)	7.96(-7)	6.48(-8)	2.69(+1)
20	2.08(+1)	2.57(-1)	1.06	7.32(-3)	7.26(-5)	7.97(-7)	7.81(-8)	2.22(+1)
30	1.27(+1)	5.15(-1)	1.08	6.41(-3)	1.40(-4)	8.77(-7)	1.08(-7)	1.43(+1)
40	6.80	7.75(-1)	1.09	5.40(-3)	2.14(-4)	1.13(-6)	1.35(-7)	8.67
50	3.44	9.89(-1)	1.10	4.47(-3)	2.80(-4)	1.60(-6)	1.51(-7)	5.54
60	2.26	1.13	1.105	3.77(-3)	3.27(-4)	2.23(-6)	1.54(-7)	4.50
70	2.35	1.17	1.10	3.48(-3)	3.49(-4)	2.88(-6)	1.42(-7)	4.62
80	2.80	1.11	1.09	3.76(-3)	3.51(-4)	3.39(-6)	1.14(-7)	4.80
90	2.72	9.73(-1)	1.075	4.79(-3)	3.46(-4)	3.62(-6)	7.65(-8)	4.78
100	1.88	7.85(-1)	1.07	6.73(-3)	3.55(-4)	3.53(-6)	5.00(-8)	3.74
110	7.07(-1)	5.82(-1)	1.08	9.67(-3)	3.99(-4)	3.21(-6)	7.62(-8)	2.38
120	9.01(-2)	4.04(-1)	1.11	1.36(-2)	4.94(-4)	2.86(-6)	2.19(-7)	1.62
130	9.30(-2)	2.86(-1)	1.17	1.83(-2)	6.44(-4)	2.70(-6)	5.45(-7)	2.41
140	3.64	2.52(-1)	1.26	2.34(-2)	8.39(-4)	2.88(-6)	1.08(-6)	5.17
150	7.85	2.99(-1)	1.36	2.84(-2)	1.05(-3)	3.40(-6)	1.79(-6)	9.54
160	1.25(+1)	3.92(-1)	1.45	3.26(-2)	1.24(-3)	4.09(-6)	2.51(-6)	1.43(+1)
170	1.60(+1)	4.79(-1)	1.53	3.53(-2)	1.38(-3)	4.68(-6)	3.07(-6)	1.80(+1)
180	1.73(+1)	5.14(-1)	1.55	3.63(-2)	1.43(-3)	4.91(-6)	3.27(-6)	1.94(+1)

Table VI. State-to-state and vibrationally elastic differential cross sections (a_0^2/sr) at selected scattering angles, using basis III and the SEPlke potential

θ	$d\sigma_{0j'}/d\Omega$							$\frac{d\sigma_0}{d\Omega}$
(deg)	j' = 0	3	4	6	7	8	9	
0	5.04(+1)	1.22(-4)	6.05(-1)	1.24(-3)	4.73(-7)	4.60(-7)	7.16(-9)	5.10(+1)
5	4.73(+1)	5.58(-3)	6.05(-1)	1.22(-3)	1.93(-6)	4.52(-7)	7.26(-9)	4.79(+1)
10	4.22(+1)	2.25(-2)	6.05(-1)	1.19(-3)	6.21(-6)	4.28(-7)	7.56(-9)	4.29(+1)
15	3.68(+1)	4.92(-2)	6.05(-1)	1.13(-3)	1.30(-5)	3.93(-7)	8.05(-9)	3.74(+1)
20	3.12(+1)	8.48(-2)	6.04(-1)	1.06(-3)	2.19(-5)	3.53(-7)	8.72(-9)	3.19(+1)
30	2.06(+1)	1.73(-1)	6.02(-1)	8.89(-4)	4.35(-5)	2.85(-7)	1.06(-8)	2.14(+1)
40	1.24(+1)	2.67(-1)	5.98(-1)	7.20(-4)	6.62(-5)	2.77(-7)	1.32(-8)	1.33(+1)
50	7.32	3.50(-1)	5.90(-1)	6.19(-4)	8.50(-5)	3.58(-7)	1.63(-8)	8.26
60	4.85	4.02(-1)	5.80(-1)	6.63(-4)	9.75(-5)	5.20(-7)	1.88(-8)	5.84
70	3.88	4.10(-1)	5.69(-1)	9.40(-4)	1.05(-4)	7.20(-7)	1.87(-8)	4.86
80	3.27	3.70(-1)	5.55(-1)	1.54(-3)	1.13(-4)	9.08(-7)	1.49(-8)	4.20
90	2.36	2.93(-1)	5.42(-1)	2.53(-3)	1.31(-4)	1.06(-6)	1.08(-8)	3.20
100	1.17	2.03(-1)	5.31(-1)	3.96(-3)	1.73(-4)	1.19(-6)	2.01(-8)	1.90
110	2.51(-1)	1.30(-1)	5.23(-1)	5.83(-3)	2.49(-4)	1.37(-6)	6.97(-8)	9.10(-1)
120	3.79(-1)	1.03(-1)	5.20(-1)	8.06(-3)	3.64(-4)	1.69(-6)	1.97(-7)	1.01
130	2.10	1.41(-1)	5.25(-1)	1.05(-2)	5.17(-4)	2.23(-6)	4.36(-7)	2.78
140	5.46	2.45(-1)	5.38(-1)	1.30(-2)	6.93(-4)	2.98(-6)	7.95(-7)	6.25
150	9.86	3.95(-1)	5.57(-1)	1.53(-2)	8.72(-4)	3.86(-6)	1.24(-6)	1.08(+1)
160	1.43(+1)	5.54(-1)	5.77(-1)	1.72(-2)	1.03(-3)	4.70(-6)	1.68(-6)	1.54(+1)
170	1.76(+1)	6.75(-1)	5.92(-1)	1.84(-2)	1.13(-3)	5.31(-6)	2.01(-6)	1.88(+1)
180	1.88(+1)	7.20(-1)	5.98(-1)	1.88(-2)	1.17(-3)	5.53(-6)	2.13(-6)	2.01(+1)

Table VII. Integral and momentum transfer state-to-state, rotationally inelastic, and vibrationally elastic cross sections (a_0^2).

	j'	SEPa			SEP1ke
		Basis I	Basis II	Basis III	Basis III
$\sigma_{0j'}$	0	5.83(+1)	5.82(+1)	5.81(+1)	8.34(+1)
	3	8.93	8.96	8.96	3.44
	4	1.42(+1)	1.42(+1)	1.42(+1)	7.00
	6	1.23(-1)	1.28(-1)	1.29(-1)	6.28(-2)
	7	5.22(-3)	5.55(-3)	5.65(-3)	3.43(-3)
	8	2.99(-5)	3.17(-5)	3.43(-5)	1.75(-5)
	9	4.29(-6)	4.60(-6)	4.94(-6)	3.03(-6)
	10	4.52(-9)	1.03(-7)	1.54(-7)	1.07(-7)
	3-10	2.32(+1)	2.33(+1)	2.33(+1)	1.05(+1)
	0-10	8.15(+1)	8.15(+1)	8.14(+1)	9.39(+1)
$\sigma^m_{0j'}$	0	4.49(+1)	4.49(+1)	4.48(+1)	5.68(+1)
	3-10	2.26(+1)	2.26(+1)	2.26(+1)	1.04(+1)
	0-10	6.75(+1)	6.75(+1)	6.74(+1)	6.72(+1)

Table VIII. Partial wave contributions, q_ℓ (a_0^2), to the integral cross sections of Table VII (Basis III).

ℓ \ j'	0	3	4	6	7	3-10	0-10
0	5.47[a]	1.24	2.97(-2)	3.15(-5)	5.60(-7)	1.27	6.74
	1.46(+1)[b]	3.88(-1)	9.82(-3)	9.88(-6)	1.40(-7)	3.98(-1)	1.50(+1)
1	1.31	1.96	5.12(-2)	5.54(-5)	1.81(-6)	2.01	3.32
	1.62(+1)	2.35(-2)	6.50(-3)	1.75(-5)	2.22(-7)	3.00(-2)	1.62(+1)
2	4.52(+1)	3.11	1.38(+1)	2.15(-2)	7.53(-4)	1.69(+1)	6.21(+1)
	4.94(+1)	1.26	6.85	1.30(-2)	4.23(-4)	8.12	5.75(+1)
3	5.00	2.52	3.18(-1)	7.89(-2)	2.35(-3)	2.92	7.92
	2.73	1.69	1.02(-1)	3.51(-2)	1.33(-3)	1.83	4.56
4	7.40(-1)	1.15(-1)	4.11(-2)	2.84(-2)	1.88(-3)	1.87(-1)	9.27(-1)
	3.32(-1)	7.28(-2)	2.92(-2)	1.45(-2)	1.27(-3)	1.18(-1)	4.50(-1)
5	2.02(-1)	1.05(-2)	1.13(-3)	1.05(-4)	6.54(-4)	1.24(-2)	2.15(-1)
	8.29(-2)	1.04(-2)	1.01(-3)	6.50(-5)	4.04(-4)	1.19(-2)	9.48(-2)
6	8.04(-2)	3.24(-3)	1.50(-4)	4.07(-5)	6.57(-6)	3.44(-3)	8.38(-2)
	3.13(-2)	2.30(-3)	1.44(-4)	3.24(-5)	2.95(-6)	2.48(-3)	3.38(-2)
7	3.45(-2)	1.07(-3)	3.71(-5)	1.32(-6)	9.50(-7)	1.11(-3)	3.56(-2)
	1.45(-2)	7.91(-4)	2.90(-5)	9.20(-7)	5.22(-7)	8.21(-4)	1.53(-2)
8	2.20(-2)	4.59(-4)	1.0(-5)	7.0(-8)	7.4(-8)	4.69(-4)	2.25(-2)
	7.65(-3)	3.56(-4)	8.0(-6)	7.0(-8)	5.4(-8)	3.64(-4)	8.02(-3)
9	1.37(-2)	2.30(-4)	3.1(-6)	4.0(-8)	1.9(-8)	2.33(-4)	1.39(-2)
	4.41(-3)	1.84(-4)	2.0(-6)	2.0(-8)	1.4(-8)	1.86(-4)	4.60(-3)
10-40	2.12(-2)	3.53(-4)	7.0(-7)	2.0(-8)	2.5(-8)	3.53(-4)	2.16(-2)
	7.59(-3)	2.99(-4)	2.0(-6)	2.0(-8)	5.0(-9)	3.01(-4)	7.89(-3)
0-40	5.81(+1)	8.96	1.42(+1)	1.29(-1)	5.65(-3)	2.33(+1)	8.14(+1)
	8.34(+1)	3.44	7.00	6.28(-2)	3.43(-3)	1.05(+1)	9.39(+1)

[a] upper entry: SEPa

[b] lower entry: SEP1ke

Table IX. Electronically and vibrationally elastic, rotationally summed integral and momentum-transfer cross sections (a_0^2) at 10 eV.

Authors	σ_0	σ_0^m	ref.
Experiment:			
Kieffer (review)	84		39
Barbarito et al.	60 ± 7[a]	...	40
Tanaka et al.	66 ± 8[b]	47 ± 6[b]	5
Theory:			
Buckingham, Massey, and Tibbs	64	c	41
Gianturco and Thompson ($r_0 = 0.84\ a_0$)	76	c	7
Present work SEPa (basis III)	81	67	...
Present work SEP1ke (basis III)	93	67	...

[a] three standard deviations of measured integral cross section

[b] propagated standard deviations of differential cross section measurements; integral cross sections then calculated by fitting, extrapolating, and integrating

[c] not available

Table X. Comparison between theoretical and experimental ratios of differential cross sections at 10 eV at different scattering angles.

Authors	$d\sigma/d\Omega(\theta) \div d\sigma/d\Omega(\theta')$				ref.
θ/θ'	30/90	40/90	60/90	60/120	
Experiment:					
Newell *et al.*	4.4	3.2	1.7	6.9	6
Tanaka *et al.*					5
measurement	3.9	3.8	1.7	5.3	
fit	4.4	3.3	2.1	6.2	
Theory:					
Gianturco & Thompson					8
$r_0 = 0.84\ a_0$	a	1.5	0.6	1.1	
$r_0 = 0.88\ a_0$	a	1.9	1.1	2.7	
$r_0 = 0.92\ a_0$	a	2.1	1.5	9.5	
Present work:					...
SEPa	3.0	1.8	0.9	2.8	
SEP1ke	6.7	4.2	1.8	5.8	

[a] not available

References

1. N. F. Lane, Rev. Mod. Phys. 52, 29 (1980).
2. P. G. Burke, N. Chandra, and F. A. Gianturco, J. Phys. B 5, 2212 (1972).
3. M. E. Riley and D. G. Truhlar, J. Chem. Phys. 63, 2182 (1975).
4. K. Rohr, J. Phys. B 13, 4897 (1980).
5. H. Tanaka, T. Okada, L. Boseten, T. Suzuki, and M. Kubo, to be published.
6. W. R. Newell, D. F. C. Brewer, and A. C. Smith, XIth Intern. Conf. Electronic and Atomic Collisions, Abstracts (Kyoto), 308 (1979).
7. F. A. Gianturco and D. G. Thompson, J. Phys. B 9, L383 (1976).
8. F. A. Gianturco and D. G. Thompson, J. Phys. B 13, 613 (1980).
9. For other recent theoretical work on e^--CH_4 scattering see (a) Z. Varga, I. Gyemant, and M. G. Benedict, Acta Physica et Chemica (Szeged, Hungary) 25, 85 (1979) and (b) S. Salvini and D. G. Thompson, J. Phys. B 14, 3797 (1981).
10. For reviews see (a) D. G. Truhlar, K. Onda, R. A. Eades, and D. A. Dixon, Int. J. Quantum Chem. Symp. 13, 601 (1979); (b) D. G. Truhlar, in Chemical Applications of Atomic and Molecular Electrostatic Potentials, edited by P. Politzer and D. G. Truhlar (Plenum, New York, 1981), p. 123. For more recent work see (c) D. Thirumalai, K. Onda, and D. G. Truhlar, J. Chem. Phys. 74, 526, 6792 (1981), and D. Thirumalai and D. G. Truhlar, J. Chem. Phys. 75, 5207 (1981).
11. S. M. Valone, D. G. Truhlar, and D. Thirumalai, Phys. Rev. A, in press.
12. T. Heil and D. Secrest, J. Chem. Phys. 69, 219 (1978); L. N. Smith and D. Secrest, J. Chem. Phys. 74, 3882 (1981).
13. A. R. Edmonds, Angular Momentum in Quantum Mechanics (Princeton University Press, Princeton, NJ, 1957). In the present article we follow the conventions of this book for all angular functions and angular momentum coupling coefficients.

14. S. L. Altman and A. P. Cracknell, Rev. Mod. Phys. 37, 19 (1965). The decomposition of the CH_4 rotational basis has also been considered by E. B. Wilson, J. Chem. Phys. 3, 276 (1935).

15. L. D. Landau and E. M. Lifshitz, Quantum Mechanics: Non-Relativistic Theory, 2nd edition (Addison-Wesley, Reading, MA, 1965), p. 362.

16. J. M. Blatt and L. C. Biedenharn, Rev. Mod. Phys. 24, 258 (1952).

17. Because of the phase convention adopted in equation (2) and for reasons discussed in D. G. Truhlar, C. A. Mead, and M. A. Brandt, Advan. Chem. Phys. 33, 296 (1975), it is appropriate to use the Z coefficients of reference 16 rather than the $\bar{Z}$ coefficients of A. M. Lane and R. G. Thomas, Rev. Mod. Phys. 30, 257 (1958).

18. K. Scanlon, R. A. Eades, D. A. Dixon, and J. Overend, J. Phys. Chem. 85, 2878 (1981).

19. S. Huzinaga, "Approximate Atomic Wavefunctions. I," Department of Chemistry Report, University of Alberta, Edmonton, Alberta, Canada, 1971.

20. F. B. van Duijneveldt, IBM Technical Research Report RJ945, No. 16437, 1971.

21. H. J. Werner and W. Meyer, Mol. Phys. 31, 855 (1976).

22. S. Huzinaga, J. Chem. Phys. 52, 1293 (1965).

23. M. Dupuis, J. Rys, and H. F. King, J. Chem. Phys. 65, 111 (1976); an earlier version of this program is available: H. King, M. Dupuis, and J. Rys, National Resource for Computation in Chemistry Software Catalog, program QH02.

24. D. B. Neumann and J. W. Moskowitz, J. Chem. Phys. 49, 2056 (1968); this program is available as part of the POLYATOM (Version II) package: D. B. Neumann, H. Basch, R. L. Kornegay, L. C. Snyder, J. W. Moskowitz, C. Hornback, and S. P. Liebman, Quantum Chemistry Program Exchange Catalog, program. no. 199.

25. D. G. Truhlar, D. A. Dixon, and R. A. Eades, J. Phys. B 12, 1913 (1979).

26. J. C. Slater and J. G. Kirkwood, Phys. Rev. 37, 682 (1931).

27. E. A. Mason and L. Monchick, Advan. Chem. Phys. 12, 329 (1967).

28. G. F. Thomas and W. J. Meath, Molec. Phys. 34, 113 (1977).

29. R. W. Kiser, Introduction to Mass Spectroscopy and Its Applications (Prentice-Hall, Englewood Cliffs, NJ, 1965), p. 314.

30. J. L. Walsh, J. H. Ahlberg, and E. N. Nilson, J. Math. Mech. 11, 225 (1962).

31. D. G. Truhlar, N. M. Harvey, K. Onda, and M. A. Brandt, in Algorithms and Computer Codes for Atomic and Molecular Scattering Theory, Vol. I, edited by L. D. Thomas (Lawrence Berkeley Laboratory, Berkeley, CA, 1979), p. 220; M. A. Brandt, D. G. Truhlar, K. Onda, and D. Thirumalai, NRCC Software Catalog (Lawrence Berkeley Laboratory, Berkeley, CA, 1980), program no. KQ12. NRCC codes are now distributed by the National Energy Software Center, Argonne National Laboratory, Argonne, IL and by the Quantum Chemistry Program Exchange, Department of Chemistry, Indiana University, Bloomington, IN.

32. G. A. Parker, B. R. Johnson, and J. C. Light, in Algorithms and Computer Codes for Atomic and Molecular Scattering Theory, Vol. II, edited by L. D. Thomas (Lawrence Berkeley Laboratory, Berkeley, CA, 1980), p. 101; G. A. Parker, B. R. Johnson, and J. C. Light, Chem. Phys. Lett. 73, 572 (1980).

33. L. D. Thomas, M. H. Alexander, B. R. Johnson, W. A. Lester, Jr., J. C. Light, K. D. McLenithan, G. A. Parker, M. J. Redmon, T. G. Schmalz, D. Secrest, and R. B. Walker, J. Comp. Phys. 41, 407 (1981).

34. G. A. Parker, J. V. Lill, and J. C. Light, NRCC Software Catalog (Lawrence Berkeley Laboratory, Berkeley, CA, 1980), program KQ04. See reference 31 for availability.

35. B. R. Johnson, J. Comp. Phys. 13, 445 (1973).

36. G. A. Parker, T. G. Schmalz, and J. C. Light, J. Chem. Phys. 73, 1757 (1980).

37. K. Onda and D. G. Truhlar, J. Chem. Phys. 69, 1361 (1978). This test case was later [K. Onda and D. G. Truhlar, J. Chem. Phys. 70, 1681 (1979)] labelled potential i for e^--N_2 scattering.

38. K. Onda and D. G. Truhlar, J. Chem. Phys. 71, 5097 (1979).

39. L. J. Kieffer, Atomic Data 2, 293 (1971) (review).

40. E. Barbarito, M. Basta, and M. Caliechio, J. Chem. Phys. 71, 54 (1979).

41. R. A. Buckingham, H. S. W. Massey, and S. R. Tibbs, Proc. Roy. Soc. London Ser. A 178, 119 (1941).

42. J. Callaway, Computer Phys. Commun. 6, 265 (1974).

Figure Captions

Figure 1. Polarization and total effective potentials for CH_4 at 10 eV as functions of the radial position of scattering electron for the relative coordinates $(\chi,\phi_\chi) = (0,0)$. Labels are as explained in the text.

Figure 2. Polarization and total effective potentials for CH_4 at 10 eV as functions of the radial position of scattering electron for the relative coordinates $(\chi,\phi_\chi) = (4\tau,0)$. Labels are as explained in the text.

Figure 3. Polarization and total effective potentials for CH_4 at 10 eV as functions of the radial position of scattering electron for the relative coordinates $(\chi,\phi_\chi) = (4\tau,60)$. Labels are as explained in the text.

Figure 4. The $\lambda = 0$ component (equivalently the spherical average) of the polarization and total effective potentials for CH_4 at 10 eV as functions of the radial position of the scattering electron. Labels are as explained in the text.

Figure 5. The first asymmetric $\lambda = 3$ component of the polarization and total effective potentials for CH_4 at 10 eV as functions of the radial position of the scattering electron. Labels are as explained in the text.

Figure 6. Differential cross sections for pure elastic scattering (labelled 0 a or 0 lke where a and lke specify which polarization potential has been used) and state-to-state rotational excitation for $j = 0 \rightarrow j' = 3$, 4, 6, and 7 as functions of the scattering angle. These cross sections were calculated with basis III.

Figure 7. Electronically and vibrationally elastic, rotationally summed differential cross sections as functions of the scattering angle for CH_4. The solid curves labelled SEPa and SEPlke represent calculations made with basis III. The dashed curve is the calculation of Gianturco et al. (reference 8) with their empirical parameter set equal to 0.88 a_0.

Figure 7 (continued)

The experimental results are shown as symbols. All results are for 10 eV except those of Gianturco and Thompson, which are for 9.5 eV.

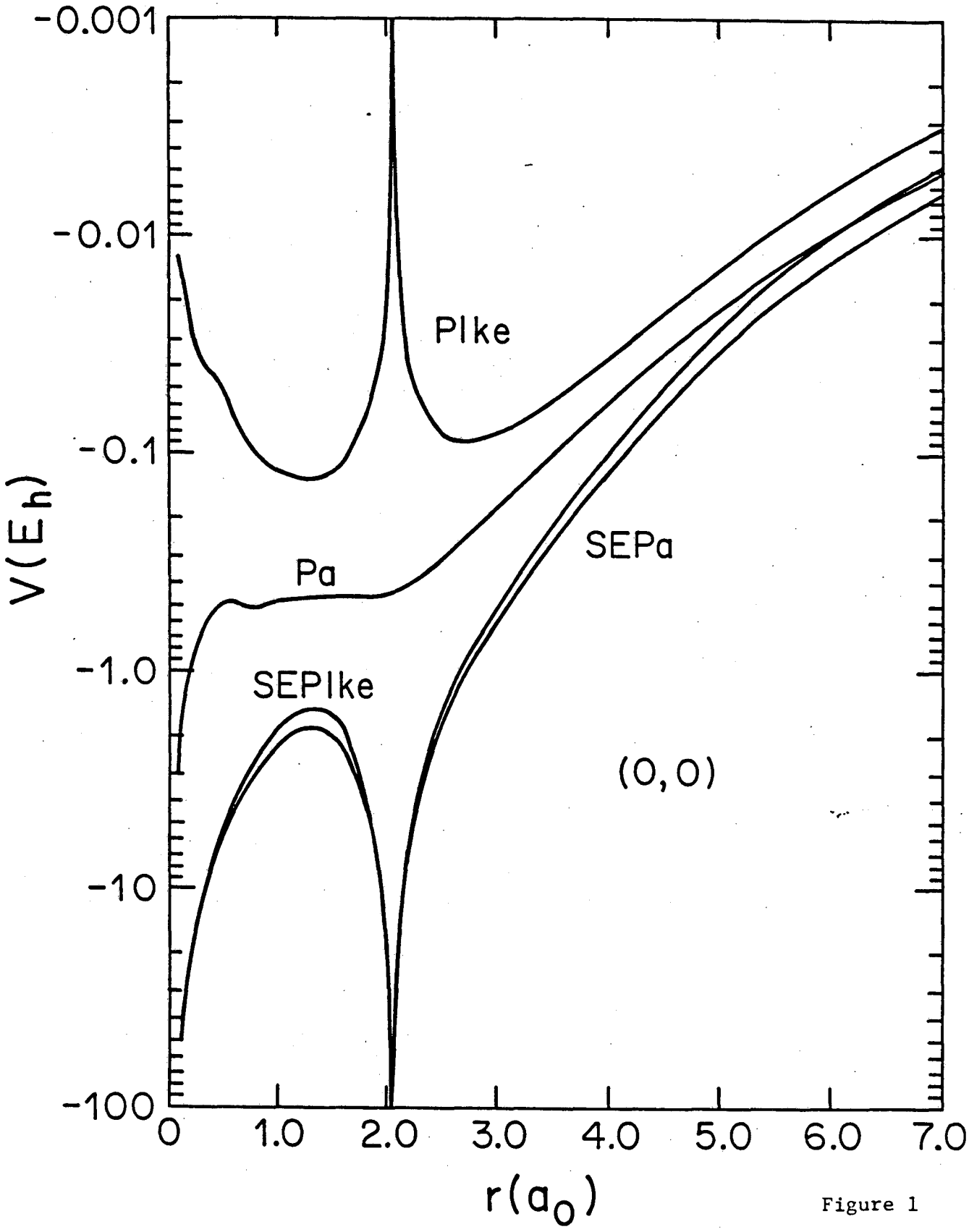
-0.001
-0.01
-0.1
-1.0
-10
-100
V(Eh)
PIke
Pa
SEPa
SEPIke
(0,0)
0
1.0
2.0
3.0
4.0
5.0
6.0
7.0
r(a0)

Figure 1

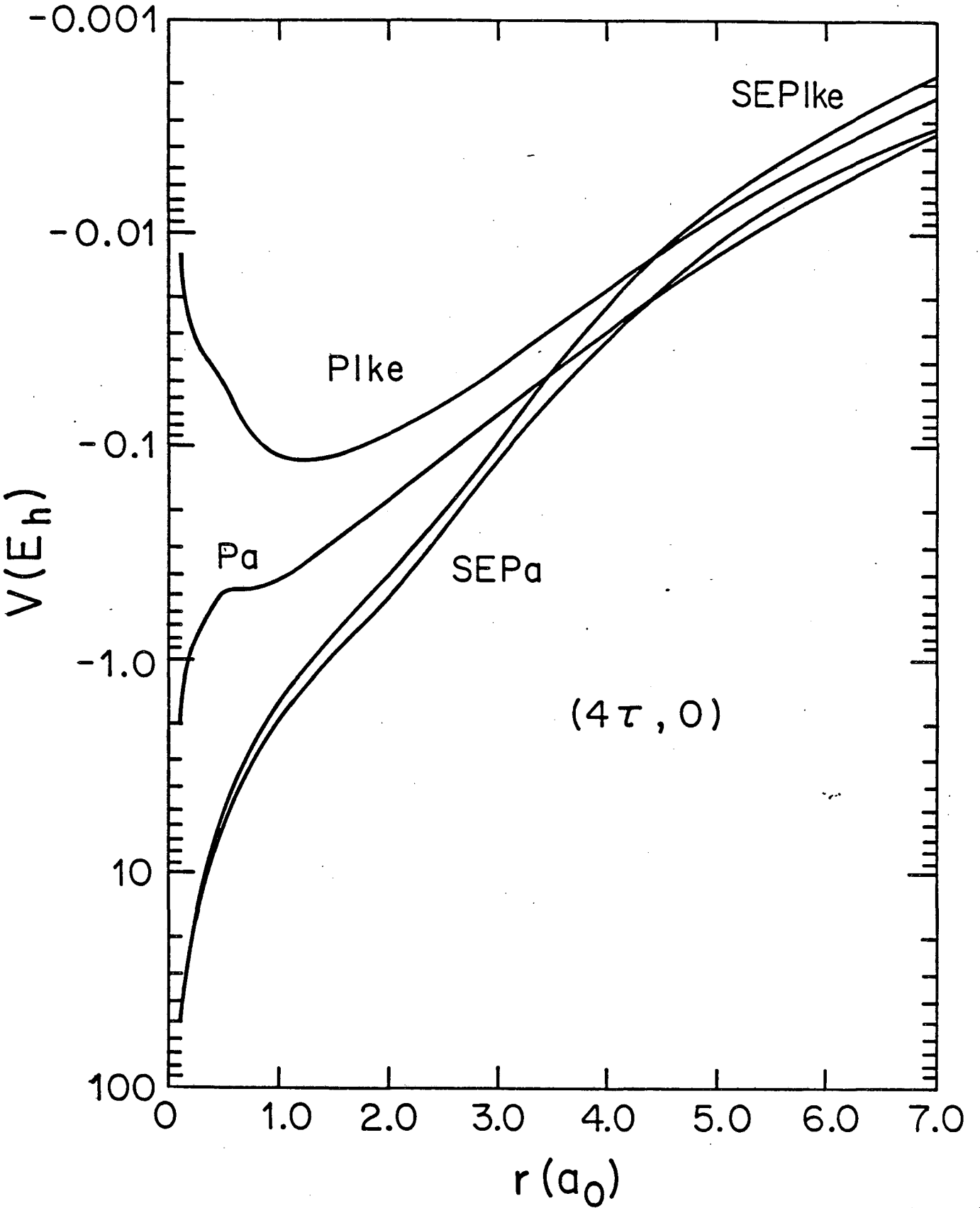
-0.001
-0.01
-0.1
-1.0
10
100
V(Eh)
SEPIke
PIke
Pa
SEPa
(4τ, 0)
0
1.0
2.0
3.0
4.0
5.0
6.0
7.0
r(a0)

Figure 2

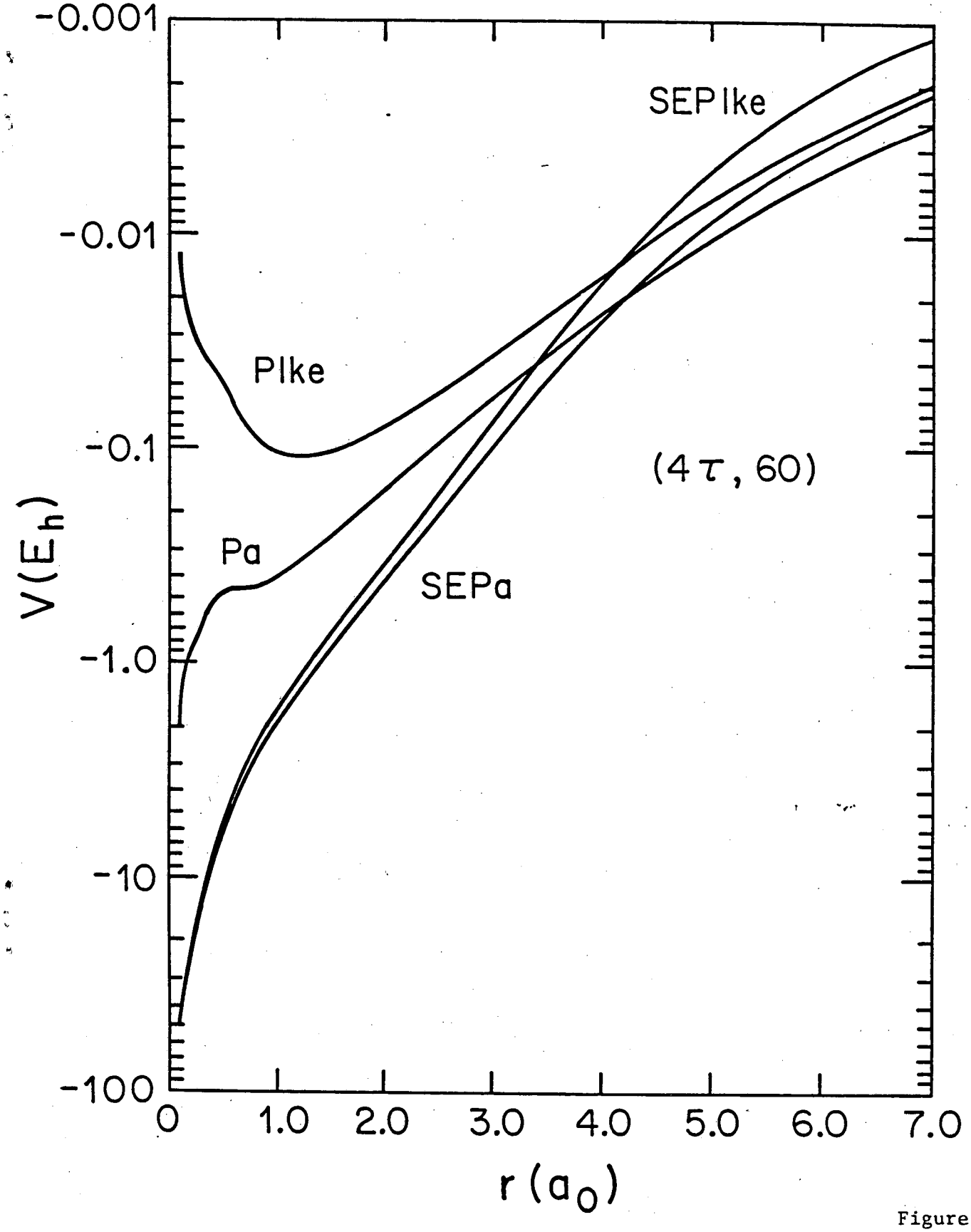
-0.001
-0.01
-0.1
-1.0
-10
-100
V(Eh)
0
1.0
2.0
3.0
4.0
5.0
6.0
7.0
r(a0)
SEPIke
PIke
Pa
SEPa
(4τ, 60)

Figure 3

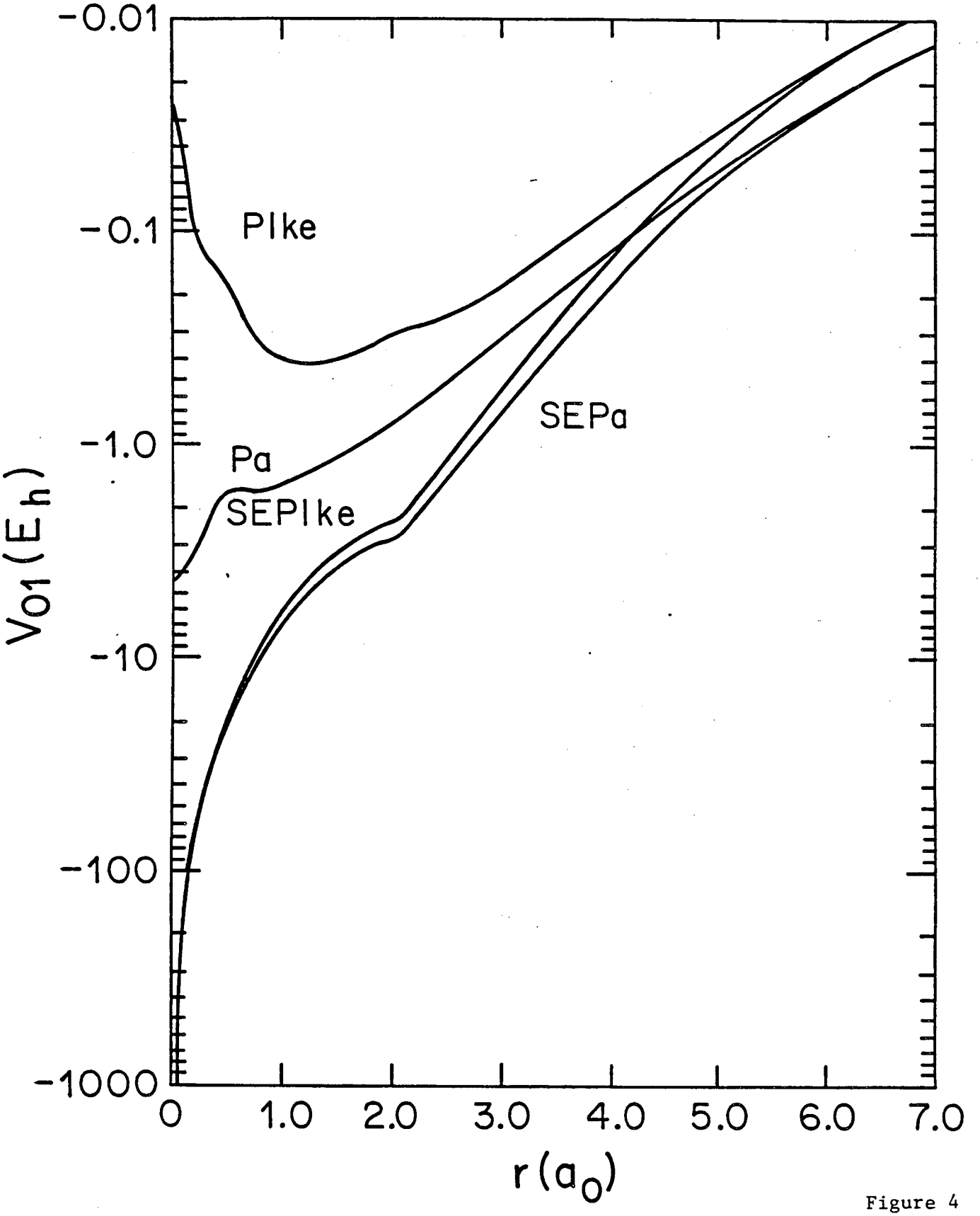
-0.01
-0.1
-1.0
-10
-100
-1000
0
1.0
2.0
3.0
4.0
5.0
6.0
7.0
$V_{01}(E_h)$
$r(a_0)$
PIke
Pa
SEPIke
SEPa

Figure 4

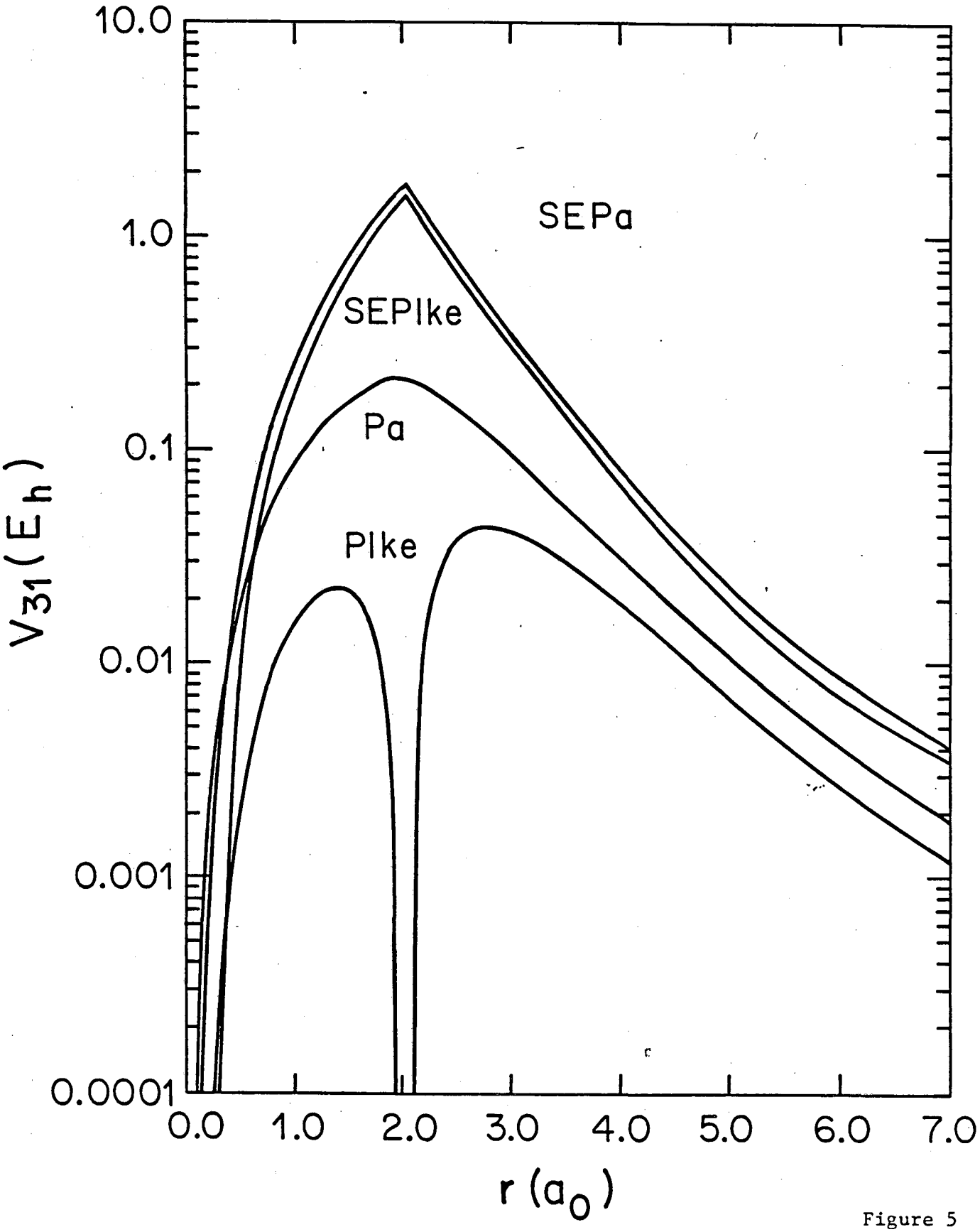
10.0
1.0
0.1
0.01
0.001
0.0001
$V_{31}(E_h)$
SEPa
SEPIke
Pa
PIke
0.0
1.0
2.0
3.0
4.0
5.0
6.0
7.0
$r(a_0)$

Figure 5

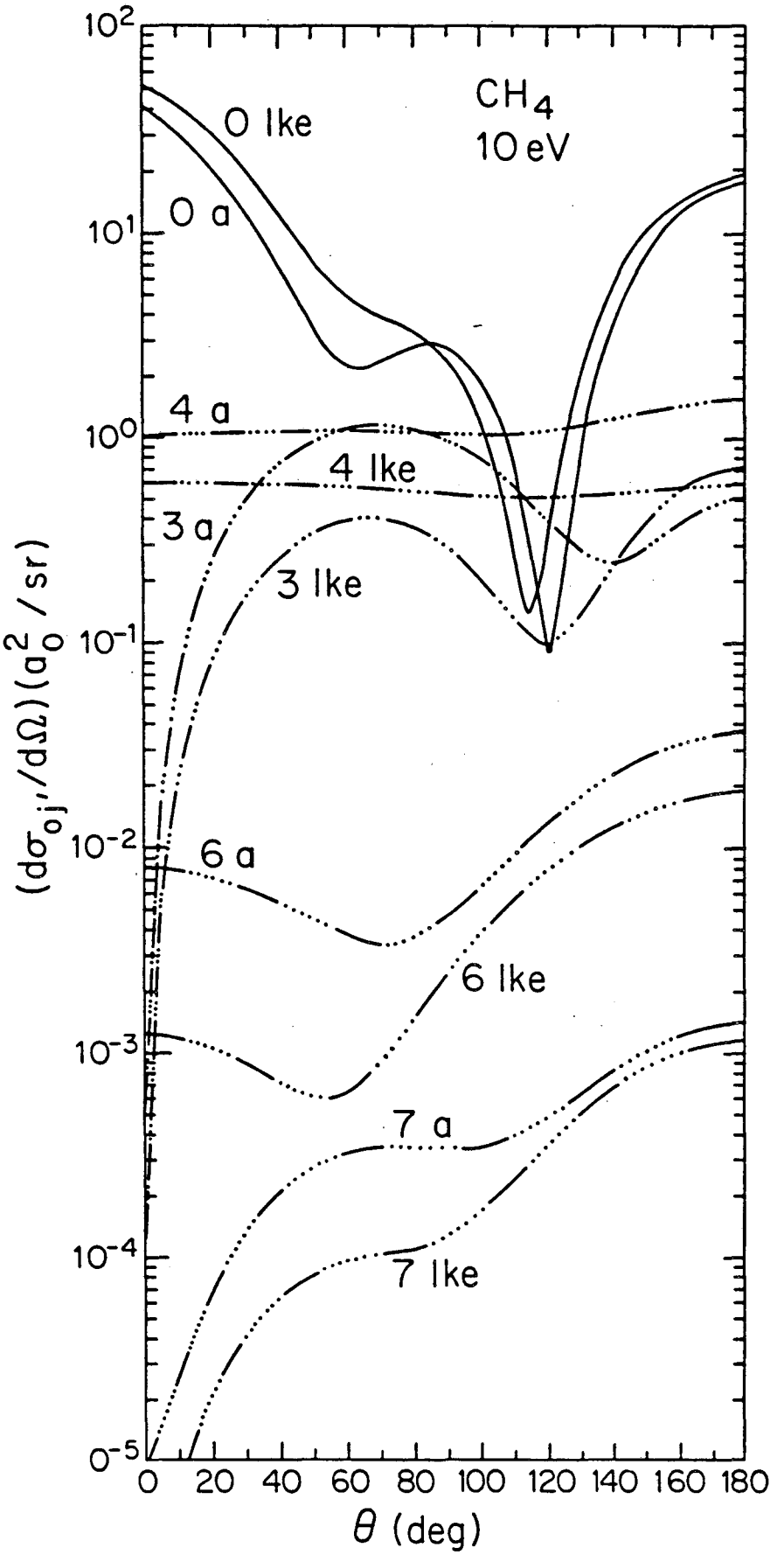
10^2
10^1
10^0
10^{-1}
10^{-2}
10^{-3}
10^{-4}
0^{-5}
CH_4
10 eV
0 Ike
0 a
4 a
4 Ike
3 a
3 Ike
6 a
6 Ike
7 a
7 Ike
$(d\sigma_{oj'}/d\Omega)(a_o^2/sr)$
0 20 40 60 80 100 120 140 160 180
θ (deg)

Figure 6

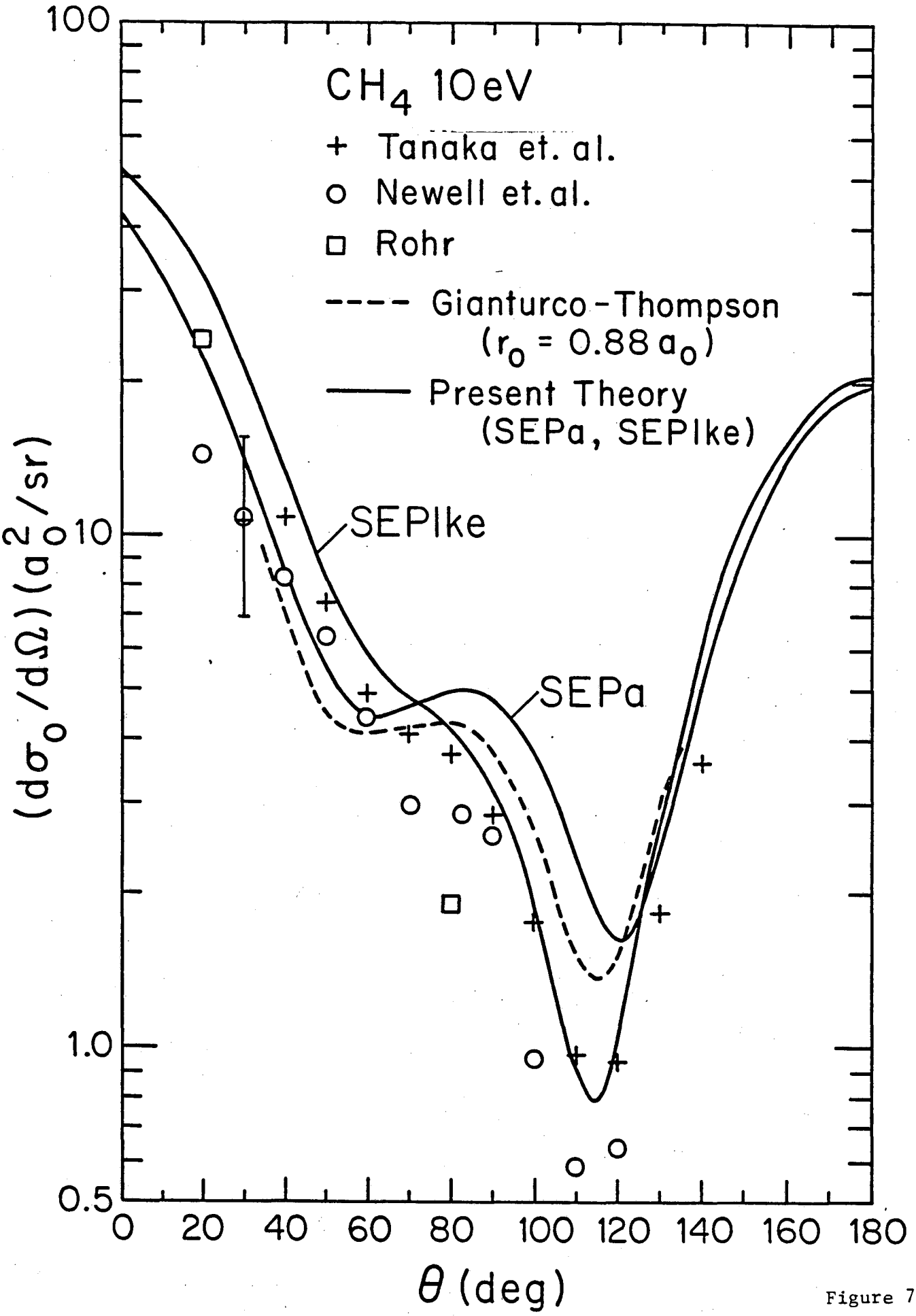
CH_4 10eV
+ Tanaka et. al.
o Newell et. al.
□ Rohr
---- Gianturco-Thompson
($r_0 = 0.88\, a_0$)
—— Present Theory
(SEPa, SEPlke)
SEPlke
SEPa
100
10
1.0
0.5
$(d\sigma_0/d\Omega)(a_0^2/sr)$
0
20
40
60
80
100
120
140
160
180
θ (deg)

Figure 7

TECHNICAL INFORMATION DEPARTMENT
LAWRENCE BERKELEY LABORATORY
UNIVERSITY OF CALIFORNIA
BERKELEY, CALIFORNIA 94720